LIBRARY
Michigan State
University

This is to certify that the
thesis entitled
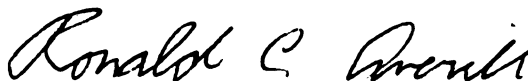
SENSITIVITY STUDY ON THE ENERGY ABSORBED
DURING A QUASI-STATIC CRUSH OF A COMPOSITE
TUBE

presented by

Narasimhan Swaminathan

has been accepted towards fulfillment
of the requirements for the

___M. S___ degree in ___Mechanical Engineering___

Ronald C. Averill
Major Professor's Signature

_12 / 8 / 03_
Date

PLACE IN RETURN BOX to remove this checkout from your record.
TO AVOID FINES return on or before date due.
MAY BE RECALLED with earlier due date if requested.

DATE DUE	DATE DUE	DATE DUE

SENSITIVITY STUDY ON THE ENERGY ABSORBED DURING A QUASI-STATIC

CRUSH OF A COMPOSITE TUBE.

By

Narasimhan Swaminathan

A THESIS

Submitted to
Michigan State University
in partial fulfillment of the requirements
for the degree of

MASTER OF SCIENCE

MECHANICAL ENGINEERING

2003

ABSTRACT

SENSITIVITY STUDY ON THE ENERGY ABSORBED DURING A QUASI-STATIC

CRUSH OF A COMPOSITE TUBE.

By

Narasimhan Swaminathan

In this work we have captured the main energy absorbing features during a tube crush experiment by simulating the same in ABAQUS/STANDARD. Mechanisms such as material failure, delamination, friction between plies and friction between the initiator and the tube are modeled and their effect on the total energy absorbed is analyzed by an ANOVA (Analysis of Variance) study. Results of such analysis may be useful in reducing cost and time in modeling, while numerically simulating a crash event for practical purposes.

Analogy between the behavior of concrete material model available in ABAQUS and failure of composite materials is used to simulate material failure. Delamination is implemented using the penalty based interface element developed as a user element subroutine. This unique interface element technology enables modeling delamination and friction between plies and hence their effect on the total energy absorbed.

Sensitivity of the response to various factors is calculated using ANOVA by taking ratio of sum of squares for an effect to the total sum of squares. Results of ANOVA concluded that delamination is an important factor and needs careful consideration for accurate numerical modeling of crash events. Sensitivity of the response to material strain energy release rate, friction and delamination related parameters were studied and it was found that material strain energy release rate and friction play a vital role in improving the response.

To my loving parents and sister.

You are only to perform your duty without an eye on their fruits.
—Gita

ACKNOWLEDGMENTS

I would like to express my sincere gratitude to my advisor Dr. Ronald C. Averill. He has motivated and guided me to the successful completion of this thesis. I would like to thank him for giving me an opportunity of being his Teaching Assistant for the graduate and undergraduate level finite element course, because of which I was able to lay a strong foundation on the fundamental concepts in the subject. I am indebted to him for the moral support that he provided during difficult times encountered, and for the time he spent with me during the course of my master's thesis. As his student I was fortunate to have an opportunity of working for his company, Red Cedar Technology, as a CPT (Curricular Practical Training) which gave me a great practical experience.

I would like to thank Dr. Dahsin Liu and Dr. Farhang Pourboghrat for being in my thesis committee and for their valuable suggestions and guidance.

I am extremely thankful to Michigan State University for having funded my Master's program through Teaching Assistantships without which I would not have been able to dedicate time and effort on this work.

I would like to thank my parents and my sister for their constant words of encouragement and support of my ideas.

Last but not least, I am thankful to all my friends and colleagues who were always of immense moral support.

TABLE OF CONTENTS

LIST OF TABLES

LIST OF FIGURES

CHAPTER 1

Introduction

1.1 Introduction

Aerospace, automobile industries and other researchers have developed various techniques to prevent damage to the passenger cell during vehicular collision. This is directly related to the energy absorption capability of the vehicle. Substantial efforts have been made to improve crash resistance in a vehicle and this is termed as crashworthiness. Crashworthiness can be achieved in two ways

1. Minimum deformation of the exposed structural member

2. Maximum deformation up to a specified limit

In the former case the frame contents may be subjected to a high level of momentum and force transfer which may be unacceptable, in the later case a large deformation in the frame is allowed and the degree of force and momentum transfer to the passenger cell is maintained within acceptable limits. This can be achieved by using energy absorption devices at strategically chosen regions of the vehicle. Since these devices undergo irreversible damage they are discarded and replaced with new ones after a crash event.

One class of energy absorption devices are structures made of materials that undergo substantial plastic deformation like steel or aluminum. During a vehicular collision, kinetic energy is used up in plastically deforming the structure and thereby reducing force and momentum transfer to the passenger cell. Another class of structures include those that

undergo fracture and other complex failure mechanisms thus using up most of the kinetic energy and maintaining acceptable limits of forces in the passenger cell.

Specially manufactured composite materials are excellent energy absorption devices. They also tend to reduce the weight of the vehicles of which they are made due a high strength to weight and stiffness to weight ratio. This has proved to be a boon in the aerospace and the automobile industry, enabling manufacturers to manufacture lighter vehicles and improve fuel economy. Composite tubes are placed at specific locations of the vehicle to absorb the impact of the collision.

Experiments involving axial crushing of composite tubes have provided useful information regarding different failure mechanisms that contribute to energy absorption capacity of composite structures. These experiments typically involve crushing a composite tube with a flat platen or an initiator. The energy absorbed is the area under the load-displacement curve.

For a general pictorial description of the crush experiment, please refer to pictures 1.1, 1.2 and 1.3. Figure 1.1 shows typical composite tubes and initiators. Figure 1.2 shows the general set up for the experiment while Figure 1.3 shows the formation of fronds and axial crack between these fronds once the tube has failed.

Unlike materials that absorb energy by plastic deformation composite materials absorb energy by a wide range of failure mechanisms and other factors like friction. Experiments involving axial crushing of tubes have brought to light different factors that contribute to energy absorption. Some of them are:

2
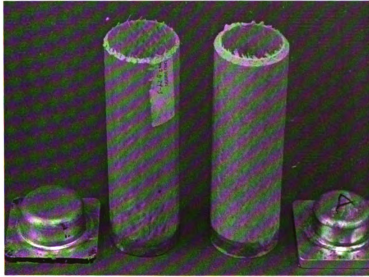
Figure 1.1: Picture showing typical composite tube and initiators
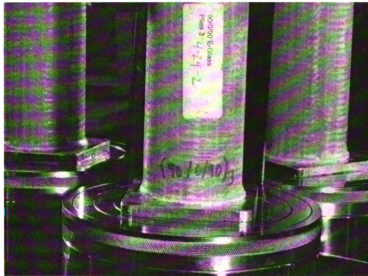
Figure 1.2: Picture showing set up for the crush experiment
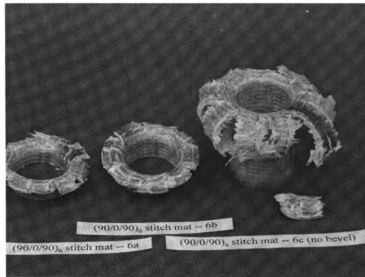
Figure 1.3: Picture showing crushed composite tubes

- Friction between the initiator and the composite structure

- Matrix deformation and failure

- Fiber failure

- Crack propagation due to Delamination

- Internal friction between failure surfaces

Each of the above mentioned factors are known to contribute to the total energy absorbed and empirical formulae have been derived to explain each of them. Though based on experimental results, it is necessary to identify the factors that contribute the most to energy absorption. This would facilitate designers, analysts and manufacturers to create better predictive models and design better crashworthy structures.

1.2 Aim of the Thesis

It is clear that a large volume of experimental results have provided researchers with useful information regarding many features of composite failure. This trend however, important, one must not overlook the importance of numerical simulation of crash events. The Finite Element Method and related software packages offer themselves as versatile tools to model and simulate a crash event and has opened new horizon to the field of numerical optimization and other sensitivity analysis. Thus numerical simulation has been able to reduce experimental testing of structures over full range of design variables, to a more fundamental level.

The aim of this thesis is to represent quasi-static axial crushing of a composite tube, and to perform a sensitivity analysis on a few parameters that have been thought to affect the energy absorption of composite tubes during a crash event. This will enable researchers to decide on certain attributes of the material while numerically simulating a crash event. It will also provide better insight into those attributes that affect energy absorption the most, or in reducing time, effort and money spent in modeling attributes whose effects can be neglected.

Analogy between the concrete material model available in ABAQUS and the failure of composite structures is implemented to simulate the axial crushing of a composite tube. This readily simulates the energy dissipated due to material failure. Delamination is implemented with the interface element that was developed for Langley research Center (NASA) by Dr. Antonio Pantano and Dr. Ronald C. Averill [1]. This unique and innovative technology simulates delamination and also enables modeling the internal friction between plies

after delamination and hence its effect on energy absorption. The interface element incorporates delamination through fracture mechanics concepts and allows for the specification for MODE I and MODE II strain energy release rates along with the corresponding strength values. This enables a study of the effect of delamination itself as a factor for the sensitivity study.

1.3 Mechanics Of Crushing

The axial crushing of the composite tube is most useful to study the mechanics of the phenomenon. A brief description of the mechanism from [2] is given as follows.

Quasi-Static Crush of a circular tube

The experiment is performed by crushing the composite tube with a steel platen (Figure 1.4). Tubes fail due to the progressive collapse and formation of continuous fronds that spread outward and inward causing a mushroom type failure. There is axial splitting that is caused by the tensile failure along the circumference (hoop direction). Initially the tube behaves elastically and the load raises to a peak value P_{max} and then drops abruptly (Figure1.5). At this stage a central intrawall crack of length L_c is formed. In the post crushing regime the load oscillates about a mean crushing load indicating progressive failure. The formation of the first peak and drop of the load is due to the formation of two equal lamina bundles, bent inward and outwards, due to flexural damage. At this stage triangular debris of pulverized material begins to form and its formation is due to the friction between the bent bundles and the steel platen. The wedge is formed when the load starts oscillating and subsequently its size remains a constant throughout the deformation process.

6

The behavior of the fibers in the tube depend on their orientation. Axially aligned fibers bend inwards or outwards, with or without fracturing, according to their flexibility. Fibers aligned in the hoop direction can only expand outwards by fracturing and inwards by either fracture or buckling.

Delamination occurs due to shear and tensile separation between plies. The axial laminae split into progressively thin layers, forming, therefore, cracks normal to the fiber direction, mainly due to fiber buckling, finally resulting either in fiber fracture or in intralaminar shear cracking which splits the laminate into many thin layers. Cracks propagate usually through the weak regions of the structure of the composite material through the resin rich regions or boundaries between the hoop fibers, resulting in their debonding, or through the interface between the hoop and axial fibers causing delamination.

1.4 Literature Review

The aim of this work is to determine the factors that contribute most to the energy absorbed during the crush of a composite tube through ANOVA (Analysis of Variance) study. It is in order to mention a few of the many works that has already been done in this field.

As the composite tube is axially crushed many energy-absorbing mechanisms are noticed and efforts have been made to predict their contribution to the total energy absorbed through experiments and empirical relationships. Significant work in this field has been done in [2,3]. Three main failure modes were identified here.
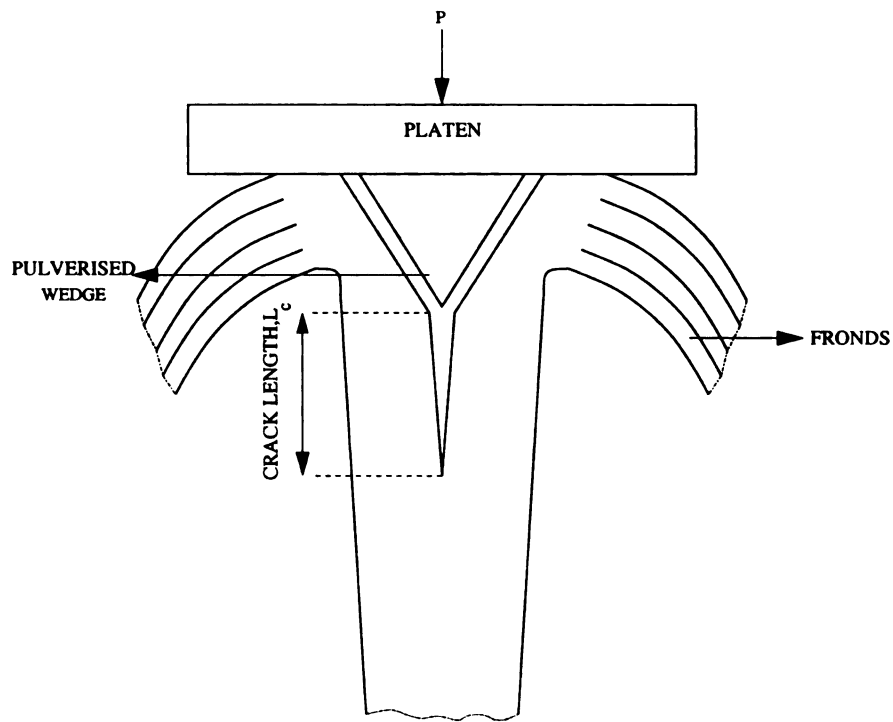
Figure 1.4: Cross Section of an Axial Crushing of a Composite Tube, From [2]
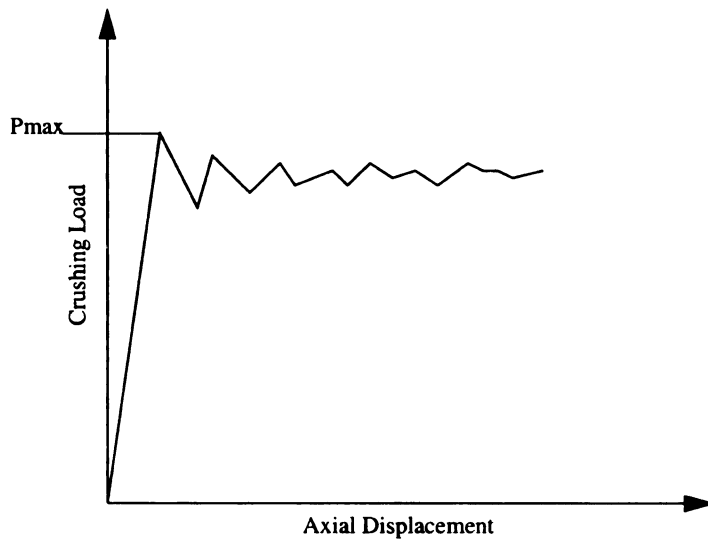
Figure 1.5: Load vs Displacement curve

1. Progressive crushing associated with large amounts of crush energy. This was called as MODE 1.

2. Brittle failure of the component resulting in catastrophic failure causing little energy absorption (MODE 2).

3. Folding and hinging similar to metal tubes with a medium energy absorption.

Experiments were performed on square tubes made of two different materials (A and B) and were crushed using a flat platen and Mode 1 and Mode 2 failure were studied. Material A was a fiber glass composite with chopped strand mat orientation in the plane of the mat and Material B was a commercial glass fiber and vinyl ester composite. Starting from the exterior of the shell, the plies were laid up in the sequence $[(90/0/2R_c)/(2R_c/0/90)/R_{c.75}]$ for material B.

Principal source of energy absorption in MODE 1 were intrawall crack propagation, bending of fronds due to cracking, axial splitting between fronds, flexural damage of plies, frictional resistance between laminates, frictional resistance due to the penetration of the debris wedge, frictional resistance of the fronds sliding along the platen.

In MODE 2 not much of energy absorption was observed as the tube collapsed due to buckling. A failure analysis was done and empirical formulae were developed to predict the energy absorbed in various failure mechanisms.

It was concluded that,

1. Energy of friction between the annular wedge and the fronds and between the fronds and the platen was estimated to be about 44% and 48% of the total, for materials A and B.

2. Energy absorbed due to bending of fronds was 48% and 32% for A and B respectively

3. Energy consumed due to crack propagation was about 7% and 18% for A and B respectively

4. Energy absorbed due to axial splitting at the four corners of square tube was 1% and 2% for A and B respectively

Haq and Newaz in [4] have studied the effect of failure modes on energy absorption in unidirectional PMC tubes. The major failure modes considered were axial cracking of tube wall, transverse cracking of fronds and delamination. Crushing standard pultruded fiberglass/polyester tubes with flat platen and initiator of two different radii performed the experiments. A hoop constraint was also used to see its effect on the peak load and hence the energy absorption. It was shown that the initiator induces a splaying crushing mode due to which a stable crushing mode is obtained. Longer the axial cracks the more compliant do the fronds become thereby not absorbing sufficient energy as they fail in buckling. The peak load was shown to be higher in case of using a flat platen than the one obtained by an initiator. It was also shown that external hoop constraint reduced the peak load and improved the sustained crushing load, avoided major transverse crack and caused delamination. It was concluded that initiation of delamination in the early stages of crushing is important to reduce the undesired high peak load value. It was also shown that the specific energy absorption in tubes increases as the radius of the initiator decreases.

In [5], test of axial splitting crush were performed on composite tubes and energy absorbing mechanisms were identified as, propagation of splitting cracks, friction, bending and delamination. Tests were performed to determine the fracture toughness, and other properties related to tension and compression. In order to evaluate energy absorption in a sharp bending due to radiussed initiator, a fixture was designed and empirical relationships were derived to find the amount of energy absorbed due to friction as a function of the bending angle. Also a formula was developed to find the load causing the axial splitting.

In their paper [6] Farley and Jones studied the effect of material and geometrical properties on the energy absorption. An equation similar to the buckling of a column was formulated for the sustained crushing load. This equation had six geometrical and material parameters associated with crushing of composite tubes, that could be useful in preliminary design and understanding the crushing behavior of composites.

In [7] it was stated that a good correlation between the experiment and the built model requires accurate representation of the structure, correct boundary conditions and the correct constitutive relationship. A fractional factorial study was done to see the effect of material properties on the energy absorption.

It was concluded in [8] that dynamic testing dissipated less energy absorption than quasi-static testing. Similar observations were recorded in [9] and it was specified that circular tubes had higher energy absorption than square tubes.
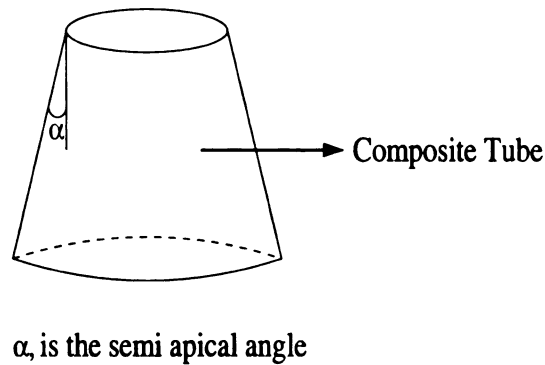
α, is the semi apical angle

Figure 1.6: Illustration of semi–apical angle

Experiments on square and circular frusta were performed in [10]. Effect of semi-apical (Figure 1.6) angle and wall thickness was studied. It was reported that increase in the semi-apical angle of the frusta tends to decrease the specific energy absorption while an increase in wall thickness tends to increase the specific energy absorption. It was also reported that specific energy absorption for circular frusta is higher that for square frusta.

In [11] crush experiments were performed on braided and CSM glass reinforced composite tubes. Initiator plug were used to initiate progressive crushing and force vs deflection curves were obtained. Analytical model for the tube crush was developed based on axisymmetric elastic deformation. The steady–state axial load was found using energy balance approach.

Composite tube crushing poses a high degree of non-linearity due to failure. Due to this, the choice of the material for numerically modeled analysis becomes an important consideration. The material model must be capable of predicting the material failure (matrix and fiber) and delamination. Bi-phase rheological models are obtained by superimposing the

effects of an orthotropic material phase and of a unidirectional material phase, the fibers. Each phase is assigned a different rheological law.

Composite materials present difficult challenges for crash modeling, this is because their failure can be attributed to many mechanisms. One of the most important issues concerning composite failure is delamination. As pointed out in [12] most common methods to model delamination are

1. Using Spot welds to represent an interface

2. Cohesive Failure Model

3. Using fracture mechanics based approaches like VCCT (Virtual Crack Closure Technique)

As pointed out in [12] the spot weld method does not have a strong physical basis, the cohesive failure model is difficult to implement and the VCCT approach, though accurate requires a high computational ability. These models are compared in [12] with MSC–Dytran and it was concluded that in computationally using these models to predict delamination the mesh size should be small and that the dynamic property data required to predict the delamination growth are not easily obtained.

In [13] a material model capable of predicting damage accumulation and braider tow scissoring was developed as a user material subroutine in ABAQUS/STANDARD. It was found that the tri-axial braid [0/±60] circular tubes exhibited crushing response that closely resembles ideal force/deflection curve. A parametric study was done and it was concluded

13

that friction played a major role and the radius of the initiator is also a crucial factor affecting the energy absorbed.

The VCCT approach was also used in [14] to determine the strain energy release rates in composite skin/stringer specimens for various combinations of uniaxial and biaxial loading conditions. A method was developed to calculate the strain energy release rates as a function of delamination lengths.

In the paper by Farley and Jones [15], the crack propagation was achieved by disconnecting the coincident nodes of the finite element. It was pointed out that for successful modeling of the energy-absorption capability, factors like crack initiation and growth, material and geometric non-linearity, fracture of individual lamina or laminae, modeling around bifurcation loads, element type and level of descretization, need to be considered.

Dr. Antonio Pantano and Dr Ronald. C Averill presented a novel interface element technology [1] for modeling delamination in composite materials and will be described in detail and also used in this work to simulate delamination.

The simulations involved in this work are implicit and quasi-static in nature and hence inertial effects are neglected. This causes serious convergence problems during the analysis and as mentioned in [16] it was required to use viscous damping that damps out the high frequency responses in the specimen.

In [17] reasons that are given for such convergence problems. In continuum based softening models used in statics is that the partial differential governing equations change from

elliptic to hyperbolic in the softening regime. Due to this, the boundary/initial conditions applicable to one class of differential equations are not appropriate to the other. As a result it is not possible for any rate-independent softening to proceed within any non-zero volume of the domain of solution [18]. Thus it is required to introduce what is known as "localization limiters". These help to resolve the mathematical ill-posedness issues that occur due to softening.

As this work involves the use of concrete material model to represent a composite structure, a reasonable understanding of numerical modeling of concrete yielding and failure was required. Literature on this was found in a consolidation of many works, in a *Report on Finite Element Analysis of reinforced Concrete* [19].

Constitutive relationships established to represent the behavior of concrete are mainly of 3 forms.

- Elasticity Based Models

- Plasticity Based models

- Plastic Fracturing Models

In the Elasticity based models the stress is a function of strain or vice-versa. This is generally expressed as

$$\sigma_{ij} = F_{ij}\varepsilon_{kl} \tag{1.1}$$

In the above equation F is a tensorial material response function and is generally a tangential or secant constitutive matrix. These models are suitable for monotonic and proportional loading and fail to predict the response correctly under unloading conditions.

The plasticity-based models assume that concrete flows on yielding and use plasticity theories like yield surfaces and flow-rules to represent the behavior. Incorporating concrete's deviations from normal metal plasticity like pressure dependent yielding and increase in volume under plastic straining (dilatancy) better represents these plastic models.

It was later investigated and concluded that plasticity models only partly represent the concrete material behavior. The fact that, under low confining pressures concrete experiences micro cracking and micro fracturing, which is accompanied by a reduction in stiffness, lead to the development of the plastic fracturing model representation. The concrete material model in ABAQUS is a **Damaged Plasticity** model and is based on the plastic fracturing theory. Further description of this model is found in the next chapter.

CHAPTER 2

Fracture Mechanics Based Material Model

2.1 MATERIAL MODEL

Composite materials are known to absorb energy through a wide range of failure mechanisms. These can be broadly classified into delamination and material failure. In the model considered for analysis both of these have been implemented. The material failure is implemented using the concrete model in ABAQUS [20], and a novel interface element technology that was developed in [1] is used to simulate delamination. In the following paragraphs detailed explanation of the concrete material model is given.

The Concrete Damaged Plasticity Material Model

It is well known that composites have in general a brittle nature. Under tensile loading the stress-strain relation is linear within the elastic limit and then material failure occurs which is due to matrix or fiber failure, or both. Under compressive loading the material behaves linearly within the elastic limit and post-elastic region in compression can be assumed to be a hardening surface (Figure 2.1). This is true because there will be load transfer across cracks formed due to compressive failure. The above-described model fits the concrete material model available in ABAQUS to model reinforced and plain concrete structures subjected to cyclic or dynamic loading under low confining pressures.

The model considers concrete as an isotropic material and hence the analogy between concrete and composite only approximately determines the material and therefore this work

17
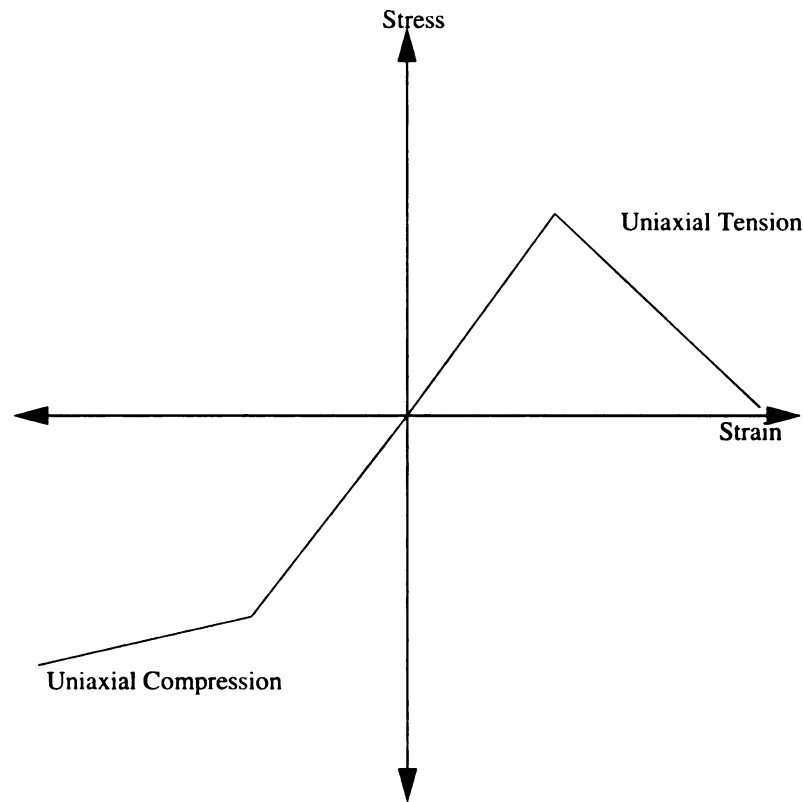
Figure 2.1: Uniaxial Tensile and Compressive behavior of a Composite

does not take into account the anisotropic nature of composite. *This sacrifice does not in any way affect the sensitivity analysis that is to be performed which is the main goal of this work.*

The Concrete material model used, as mentioned previously is a damaged plasticity model. It is most convenient to describe and understand the model with the appropriate keywords that is used to implement the model in ABAQUS (Please see [20]). Fundamental concepts and theory are also explained with the keywords. The model is implemented using the following keywords.

- *ELASTIC

- *CONCRETE DAMAGED PLASTICITY

- *CONCRETE TENSION STIFFENING

- *CONCRETE COMPRESSION HARDENING

- *CONCRETE TENSION DAMAGE

- *CONCRETE COMPRESSION DAMAGE

2.1.1 *ELASTIC

This keyword specifies the elastic properties of the isotropic material. The Young's modulus and poisson's ratio form the data card to this keyword.

2.1.2 *CONCRETE DAMAGED PLASTICITY

The Concrete damaged plasticity model in ABAQUS uses concepts of isotropic damaged elasticity along with isotropic tensile and compressive plasticity to represent the inelastic behavior of concrete. The keyword is used to define the flow potential, yield surface and viscosity parameters. The various data card to be mentioned for the keyword are:

- Dilation angle, ψ: Dilation angle , in degrees in the $p - q$ plane (p - First invariant of the stress tensor, q- Von-Mises equivalent deviatoric stress, see Figure 2.2). Dilatancy is a concept applicable to brittle materials that represents an increase in the volume on undergoing inelastic strains. This is mainly due to the formation of microcracks. The term *dilatancy* has in general not known to be applied for composite failure and
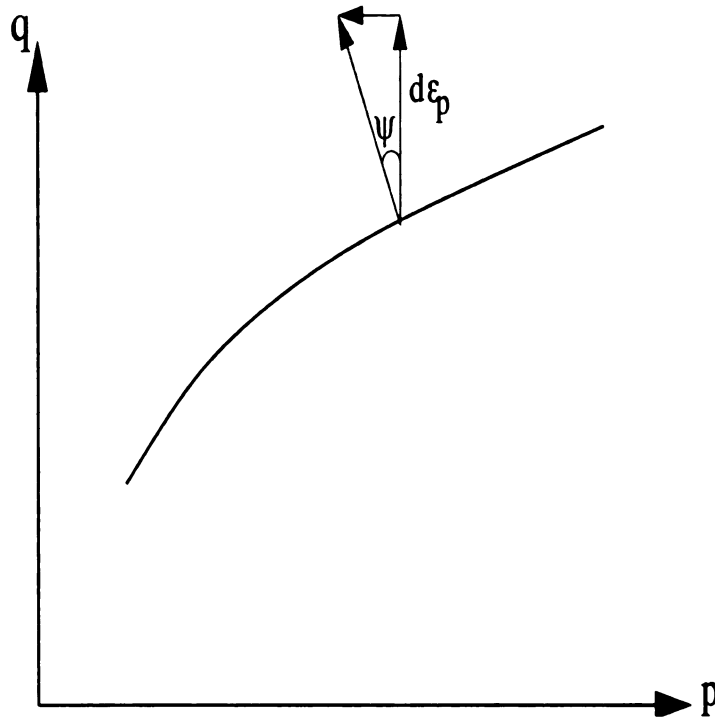
Figure 2.2: Illustration of Dilatation angle

for all analyses considered it is given a value of 30°.

- Flow potential eccentricity: A flow potential describes the accumulation of plastic strain as the body undergoes plastic deformation. This model uses the Drucker-Prager flow potential function and requires a small positive number representing the flow potential eccentricity at which the hyperbolic flow potential approaches an asymptote. The default is 0.1.

- Ratio of initial equi-axial compressive yield stress to the initial uniaxial compressive yield stress: This data specifies the yield surface and has a default value of 1.16. This

value remains as a default for this analysis.

- K_C: This value represents the ratio of the second stress invariant on the tensile meridian to that on the compressive meridian at initial yield for any given value of the pressure invariant such that the maximum principal stress is negative. The default value of $\frac{2}{3}$ is used.

- Viscosity parameter μ: is used for the viscoplastic regularization of the concrete constitutive equations. This is given a value of $1E - 4$ to facilitate numerical convergence. Please see [17,18,20–23] for further details on the purpose of using this value.

2.1.3   *CONCRETE TENSION STIFFENING

When both concrete and the reinforcement are subjected to tensile stresses, large cracks form in concrete. The bond failure between the reinforcement and concrete matrix also occur at the same time and relative movement between reinforcement and concrete takes place. The shear forces at the contact feed tension stresses to the concrete between the cracks. The concrete hangs on the structure and contributes to the overall stiffness of the structure. This is referred to as *tension stiffening*.

The post failure region is modeled so that the stress decreases gradually from the ultimate tensile stress to zero. This describes the cracks as cohesive cracks; this means that the cracks are capable of transferring stress. This may be a valid assumption in case of composite structures also, because there is definitely stress transfer by the interlocking fibers

as the matrix fails. The cracking model is a smeared cracking model. This means that at a point when stress reaches the crack detection surface the crack is accounted by the way in which it affects the stress distribution in the structure. Cracks are assumed to occur parallel to each other in a finite element and this is numerically modeled by reducing the stiffness in a direction perpendicular to the crack [18]. ABAQUS offers three ways to specify the post failure region. These are available as options under the *CONCRETE TENSION STIFFENING keyword.

- TYPE=STRAIN: The first one is TYPE=STRAIN option (Figure 2.3). This gives the post failure stress as a function of cracking strain across the crack. This approach is in general both physically and computationally unacceptable due to following reasons described in [18].

  - The softening zone has zero volume and width.

  - The inelastic strain and fracture work are zero.

  - The solutions are un-objective. This means that the results do not converge to a unique value as the mesh is refined. This is due the formation of narrower crack bands and localization of strains.

  Due to these disadvantages this method of specification was not used in the current model. Please refer to [18] for more information.

- TYPE=DISPLACEMENT: This option overcomes the disadvantages of the previous option. Here the stress is a function of the crack opening displacement rather that the cracking strain (Figure 2.4). This method of defining the post failure region belong to the crack band models and are acceptable both physically and computationally.
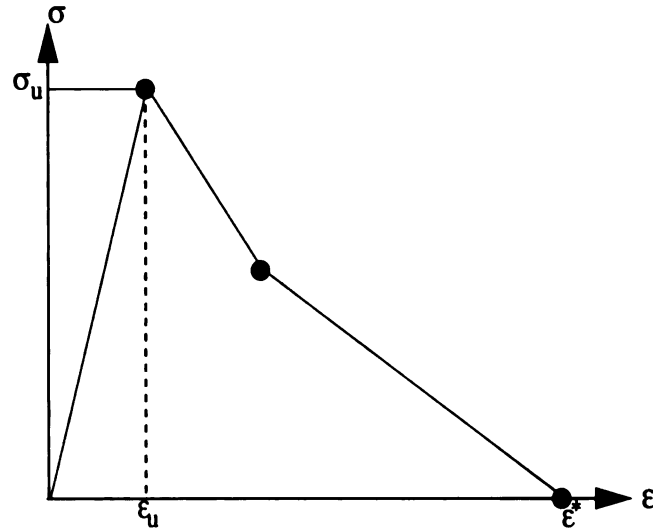
Figure 2.3: Tension Stiffening, (Type= Strain, option)

The option is based on the model developed by Hillerborg in, [24]. It is based on the assumption that the stress across the crack does not go to zero as long as the crack is narrow. The data card that needs to be given for this option is the crack opening displacement or the width of the crack at which the stress linearly decreases to zero. The model can be easily calibrated for the current model by knowing the value of the strain energy release rate for the material. Before describing the Hillerborg's model a few failure theories from fracture mechanics are in order.

2.1.4 Fracture Mechanics

Many theories have been developed that are used to predict the formation and propagation of cracks and to simulate them using Finite Element Method. Fracture mechanics generally predicts material failure and crack propagation using energy based

approach.

Stress intensity factor approach.

In this theory the stresses in the crack tip theoretically approach infinity according to the expression $\sigma = K/\sqrt{2\pi r}$ where r is the distance from the crack tip and K is the stress intensity factor that depends on load and crack geometry. Once K reaches a critical value of K_c called the critical stress intensity factor, the crack grows. Using this method along with FEM to predict crack propagation requires finer mesh at the crack tip. This limits its application to complicated problems.

Energy Balance Approach

This was the model originally developed by Griffith. He concluded that the energy G_c required to create free surfaces in a body was in general a material constant this is given as the energy required to produce a unit area of crack in a material.

When work is done to deform a material a part of the energy is stored as elastic strain energy and the remaining is available for forming free surfaces. If W is the external work done and U is the strain energy stored, then $W - U$ is available to form free surface. If $W - U$ is equal to G_c * (free area produced due to crack) then the crack propagates quasi-statically (refer to [18]).
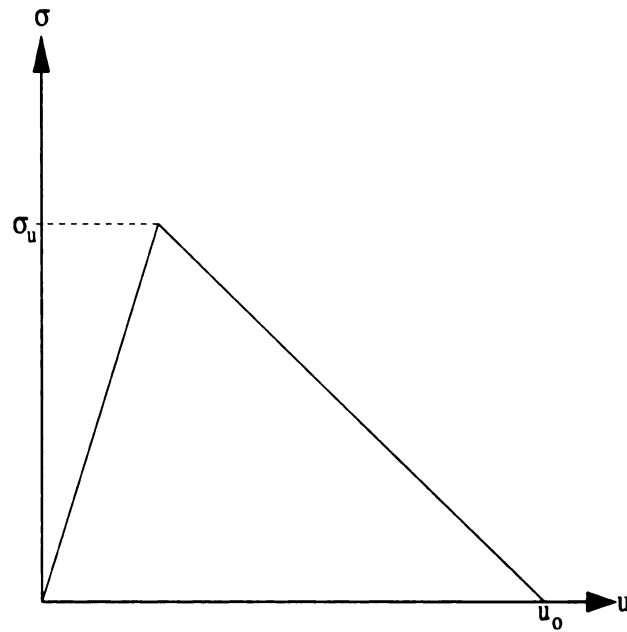
Figure 2.4: Tension Stiffening, (Type=Displacement)

Hillerborg's Model

In the Hillerborg's model the stress does not go to zero as long as the crack is narrow, the limit being given by the crack opening displacement u_0. Figure 2.4 illustrates the model.

So the amount of energy required to open a unit area of this crack is given by

$$\frac{1}{2}\sigma_u u_0 \qquad (2.1)$$

This energy can be equated to the strain energy release rate G_c of the material to obtain the crack opening displacement.

25

The distribution of the stress as a function of the crack opening displacement can be assumed to be linear for brittle materials like concrete and composites

For a linear relationship we therefore have

$$\frac{1}{2}\sigma_u u_0 = G_c \tag{2.2}$$

$$u_0 = 2\frac{G_c}{\sigma_u} \tag{2.3}$$

- TYPE=GFI: This option is the same as the TYPE=DISPLACEMENT option, except that one can directly specify the strain energy release rate for the ultimate tensile strength. This option has been used for all analysis in this work . The specification of the strain energy release rate is independent on size of the finite element and hence overcomes the disadvantages of strain localization and mesh dependency of the results.

Consider a square finite element of dimension l by l as illustrated in Figure 2.5. The stress in the element reaches maximum value at a strain value of ε_f. The stress then decreases to zero at a strain of $10\varepsilon_f$. After failure the finite element is in two pieces separated by a crack of dimension $10\varepsilon_f l = u_0$. Thus we have converted the strain value to a crack opening displacement assuming that the inelastic strain in the two pieces in negligible. The strain energy release rate can be calculated according to Hillerborg, [24] as

$$\frac{1}{2}\sigma_u u_0 = G_c \tag{2.4}$$

Specifying the strain energy release rate in this way resolves the illposedness is-
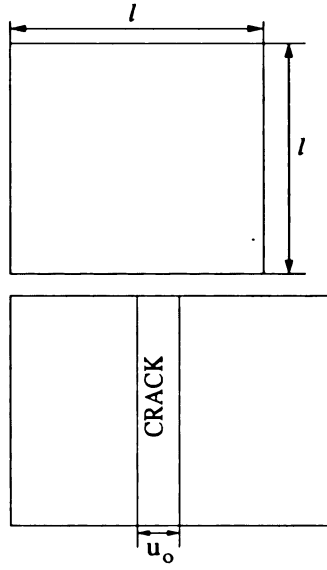
Figure 2.5: Figure Illustrating the size effect of fracture energy

sues of the governing partial differential equations to a certain extent. This is true because the crack no longer localizes on to a point but to a characteristic dimension in the specimen. This is therefore a kind of "localization limiter". Please refer to [17, 18, 20] for more detailed mathematical explanation. The specification of the *Stress-Crack opening Displacement* or the *Stress–Strain Energy release rate* is mesh objective. This however modifies the plastic modulus of the *stress-strain* diagram as the mesh descretization is changed.

For the current work the value "10" will be reffered to as **Strain Ratio** (SR) . It is the ratio between the strain at complete loss of strength to the strain at failure. This ratio will be considered to be a factor that affects the response.The strain energy release rate is dependent on the strain ratio through the expression

27

-ε

E

-σ
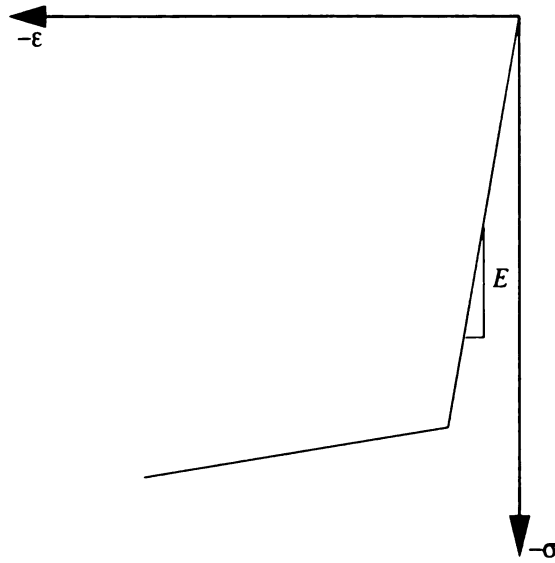
Figure 2.6: Simple Linear Hardening in Compression

$$G_c = \frac{1}{2}\sigma_u(l)(SR)\varepsilon_f \qquad (2.5)$$

2.1.5 *COMPRESSION HARDENING

This keyword is used to specify the hardening behavior of concrete in compression. It requires the specification of maximum stress in compression as a function of inelastic strain. For the sake of simplicity a linear hardening is assumed after maximum stress in compression is reached. Please see Figure 2.6.

2.1.6 *CONCRETE TENSION DAMAGE

This keyword specifies the decrease in elastic stiffness as the stress decreases to zero. The degradation of stiffness increases with increase in plastic strain. This specification

28
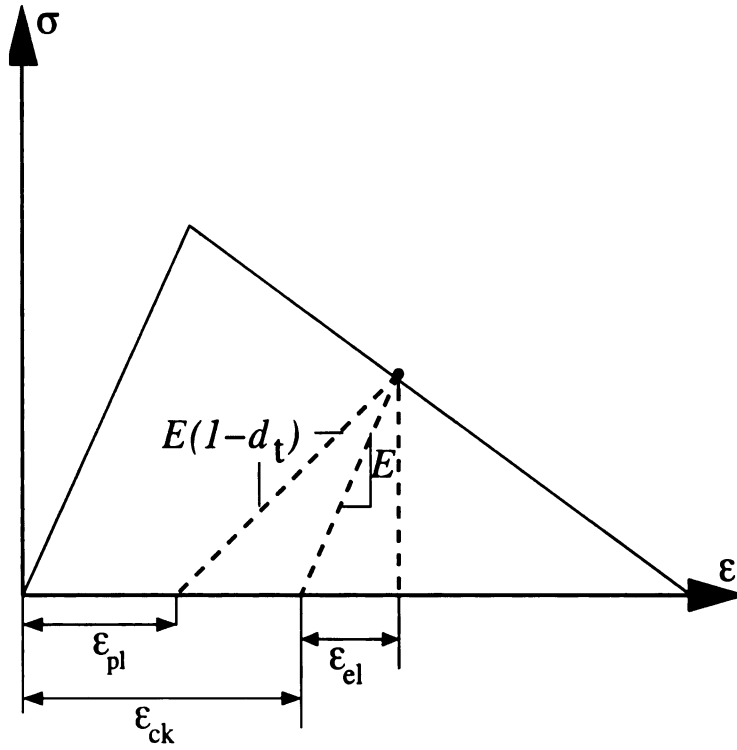
Figure 2.7: Illustration of Damage Material Model

adds plasticity to the model and is governed by scalar damaged elasticity as shown in Figure 2.7. The undamaged inelastic strain is decomposed into plastic strain and cracking strain. The data is mentioned by specifying the scalar damage variable ($0 \leq d \leq 1$) as a function cracking strain (ε_{ck}). This is not used in the current research, due to difficulty in obtaining the softening data. This keyword also has the option to specify the compression stiffness recovery ($0 \leq w_c \leq 1$) that may be required if loading is cyclic.

2.1.7 *CONCRETE COMPRESSION DAMAGE

Similar to the tension damage, the model also allows modeling crushing in concrete by stiffness degradation. Option for tension stiffness recovery is also provided to enable modeling cyclic loading. This is not used in this model due to difficulty in specification of softening data. The specification of this may lead to convergence difficulties due to decrease in stiffness during compression.

CHAPTER 3

Interface Element Technology

3.1 Modeling Delamination

The interface element developed to join independently modeled finite element meshes and simulate delamination in composite structures has been used to incorporate delamination, [1]. The interface element is a penalty-based model, this means that the constraints are enforced through a penalty parameter. A brief description of the interface element and its method of specification for the model are in order.

The motivation to develop the interface element based on penalty method comes from the Lagrange multiplier method, which is described below.

The following examples from [25] illustrates the two methods.

Lagrange Multiplier Method

Consider the minimization of a function $f(x,y) = 4x^2 - 3y^2 + 2xy + 6x - 3y + 5$ subject to the constraint $G(x,y) = 2x + 3y = 0$. Using the Lagrange multiplier method the equation is $F_L(x,y) = f(x,y) + \lambda(2x + 3y)$, by taking the partial derivative of this equation with respect to x, y, and λ and equating to zero, three equations are obtained that can be solved for x, y and λ.

$$\frac{\partial F_L}{\partial x} = 8x + 2y + 6 + 2\lambda = 0 \tag{3.1}$$

31

$$\frac{\partial F_L}{\partial y} = -6y + 2x - 3 + 3\lambda = 0 \qquad (3.2)$$

$$\frac{\partial F_L}{\partial \lambda} = 2x + 3y = 0 \qquad (3.3)$$

This gives $x = -3$, $y = 2$ and $\lambda = 7$.

Penalty method

Consider the minimization of the same function, using the penalty method we consider the equation in the following manner, $F_P(x,y) = f(x,y) + \frac{\gamma}{2}(2x + 3y)^2$. By differentiating this equation with x, y and equating to zero we get x and y in terms of the penalty parameter.

$$\frac{\partial F_P}{\partial x} = 8x + 2y + 6 + 2\gamma(2x + 3y) = 0 \qquad (3.4)$$

$$\frac{\partial F_P}{\partial y} = -6y + 2x - 3 + 3\gamma(2x + 3y) = 0 \qquad (3.5)$$

This gives $x = \frac{15 - 36\gamma}{-26 + 12\gamma}$ and $y = \frac{18 + 24\gamma}{-26 + 12\gamma}$ and clearly as $\gamma \to \infty$ the value of x and y reach the value given by Lagrange multiplier method and this also happens to be the exact solution to the problem. Though the accuracy of the problem depends on the value chosen for γ when used in finite element method or the potential energy method this greatly reduces the size of the stiffness matrix.

A high value of γ predicts results more accurately. The reduction in the size of the matrix results because the function is not differentiated with respect to the penalty parameter and hence there is lesser number of primary degrees of freedom to solve for, unlike the Lagrange multiplier method. Lagrange multiplier method does in fact impose the constraints accurately and hence serves as a limit to the accuracy of finite element solutions obtained

32

by the penalty method.

3.2 Application of Penalty and Lagrange multiplier method

Consider a problem of an axial load applied to a bar. To solve this problem the Total potential energy (TPE) of the bar is developed as the sum of the strain energy and the work done by external forces. We have for a bar of length l acted upon by external forces, the potential energy is given by:

$$\Pi_1 = \frac{1}{2} \int_0^l EA\left(\frac{du}{dx}\right)^2 dx - f_i u_i \tag{3.6}$$

, where E is the Young's modulus, A the area of cross section and u the displacement as a function of x, f_i the applied external forces on the nodes and the corresponding displacements. Now consider two elements of the bar, each of length l joined together at the node as in Figure 3.1

The TPE of the bar will alone be

$$\Pi_1 = \frac{1}{2} \int_0^l EA\left(\frac{du}{dx}\right)^2 dx + \frac{1}{2} \int_l^{2l} EA\left(\frac{du}{dx}\right)^2 dx - \sum_{i=1}^4 f_i u_i \tag{3.7}$$

In ordinary problems this functional is minimized after substituting approximate functions, for the displacement field, u. Now, if we have the interface element, which has its own displacement field V, connecting the two bar elements, the potential energy of the bar is subjected to two constraints $V - u_2 = 0$ and $V - u_3 = 0$ where u_2 and u_3 are the global primary degrees of freedom for the second node of the first bar element and first node of the
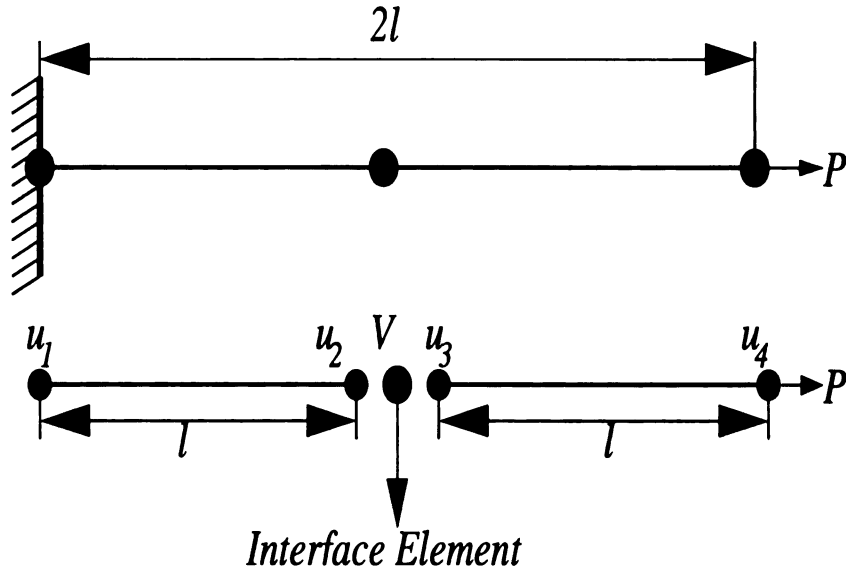
Figure 3.1: Application of Lagrange Multiplier method to a bar problem

second bar element. Thus in using the Lagrange multiplier method to minimize the TPE subject to the constraints specified we have the TPE of the system to be

$$\Pi = \frac{1}{2}\int_0^l EA\left(\frac{du}{dx}\right)^2 dx + \frac{1}{2}\int_l^{2l} EA\left(\frac{du}{dx}\right)^2 dx - \sum_{i=1}^4 f_i u_i + \lambda_1(V - u_2) + \lambda_2(V - u_3) \quad (3.8)$$

Now to solve this problem we first replace u with its approximation functions. Using Lagrange interpolation functions we have

$$u = \sum_{j=1}^2 u_j \psi_j \quad (3.9)$$

$$or \quad (3.10)$$

$$u_1\left(1 - \frac{x}{l}\right) + u_2\left(\frac{x}{l}\right) \quad (3.11)$$

34

Thus substituting for u we get

$$\Pi = \frac{E_1 A_1}{2} \int_0^l \left(\sum_{i=1}^2 u_i \frac{d\psi_i}{dx} \right) \left(\sum_{j=1}^2 u_j \frac{d\psi_j}{dx} dx \right) + \frac{E_2 A_2}{2} \int_l^{2l} \left(\sum_{i=1}^2 u_i \frac{d\psi_i}{dx} \right) \left(\sum_{j=1}^2 u_j \frac{d\psi_j}{dx} \right) dx$$

(3.12)

$$-Pu_4 + \lambda_1 (V - u_2) + \lambda_2 (V - u_3)$$

Now taking partial derivative with respect to $u_1, u_2, u_3, u_4, V, \lambda_1, \lambda_2$ and equating to zero, we will get a FE model that has 7 equations in seven variables looking like

$$
\begin{pmatrix}
\frac{E_1 A_1}{l} & -\frac{E_1 A_1}{l} & 0 & 0 & 0 & 0 & 0 \\
-\frac{E_1 A_1}{l} & \frac{E_1 A_1}{l} & 0 & 0 & 0 & -1 & 0 \\
0 & 0 & \frac{E_2 A_2}{l} & -\frac{E_2 A_2}{l} & 0 & 0 & -1 \\
0 & 0 & -\frac{E_2 A_2}{l} & \frac{E_2 A_2}{l} & 0 & 0 & 0 \\
0 & 0 & 0 & 0 & 0 & 1 & 1 \\
0 & -1 & 0 & 0 & 1 & 0 & 0 \\
0 & 0 & -1 & 0 & 1 & 0 & 0
\end{pmatrix}
\begin{pmatrix}
0 \\
u_2 \\
u_3 \\
u_4 \\
V \\
\lambda_1 \\
\lambda_2
\end{pmatrix}
=
\begin{pmatrix}
f_1 \\
0 \\
0 \\
P \\
0 \\
0 \\
0
\end{pmatrix}
$$

(3.13)

Clearly the above system is symmetric, banded and not positive definite. Solving we get,

$$f_1 = P \qquad (3.14)$$

$$\lambda_1 = P \qquad (3.15)$$

$$\lambda_2 = -P \qquad (3.16)$$

$$u_2 = u_3 = V = \frac{Pl}{E_1 A_1} \qquad (3.17)$$

$$u_4 = \frac{Pl}{E_1 A_1} + \frac{Pl}{E_2 A_2} \qquad (3.18)$$

Now we do the same thing using two penalty parameters to impose the constraints

$$\Pi = \frac{E_1 A_1}{2} \int_0^l \left(\sum_{i=1}^2 u_i \frac{d\psi_i}{dx} \right) \left(\sum_{j=1}^2 u_j \frac{d\psi_j}{dx} dx \right) + \frac{E_2 A_2}{2} \int_l^{2l} \left(\sum_{i=1}^2 u_i \frac{d\psi_i}{dx} \right) \left(\sum_{j=1}^2 u_j \frac{d\psi_j}{dx} \right) dx$$

$$-Pu_4 + \frac{\gamma_1}{2}(V - u_2)^2 + \frac{\gamma_2}{2}(V - u_3)^2 \tag{3.19}$$

Partially differentiating the above equation with respect to u_1, u_2, u_3, u_4 and V we get 5 equations and the FE model looks like

$$
\begin{pmatrix}
\frac{E_1 A_1}{l} & -\frac{E_1 A_1}{l} & 0 & 0 & 0 \\
-\frac{E_1 A_1}{l} & \frac{E_1 A_1}{l} + \gamma_1 & 0 & 0 & -\gamma_1 \\
0 & 0 & \frac{E_2 A_2}{l} + \gamma_2 & -\frac{E_2 A_2}{l} & -\gamma_2 \\
0 & 0 & -\frac{E_2 A_2}{l} & \frac{E_2 A_2}{l} & 0 \\
0 & -\gamma_1 & -\gamma_2 & 0 & \gamma_1 + \gamma_2
\end{pmatrix}
\begin{pmatrix}
0 \\ u_2 \\ u_3 \\ u_4 \\ V
\end{pmatrix}
=
\begin{pmatrix}
f_1 \\ 0 \\ 0 \\ P \\ 0
\end{pmatrix}
\tag{3.20}
$$

The above matrix is symmetric, banded, sparse and also positive definite after applying the boundary conditions. Solving, we get

$$f_1 = -P \tag{3.21}$$

$$u_2 = \frac{Pl}{E_1 A_1} \tag{3.22}$$

$$V = \left(\frac{1}{\gamma_1} + \frac{l}{E_1 A_1} \right) P \tag{3.23}$$

$$u_3 = \left(\frac{l}{E_1 A_1} + \frac{1}{\gamma_1} + \frac{1}{\gamma_2} \right) P \tag{3.24}$$

$$u_4 = \left(\frac{l}{E_1 A_1} + \frac{1}{\gamma_1} \right) P + \left(\frac{l}{E_2 A_2} + \frac{1}{\gamma_2} \right) P \tag{3.25}$$

And as γ_1 and γ_2 tend to infinity the values u_3, V and u_4 take values obtained using the Lagrange multiplier method. Thus the Lagrange multiplier method sets the limit of accuracy obtained using the penalty method. Dividing the solutions obtained from the Lagrange multiplier and the penalty method for u_4 we get

36

$$\frac{u_4^{penalty}}{u_4^{lagrange}} = 1 + \frac{\frac{1}{\gamma_1} + \frac{1}{\gamma_2}}{\frac{l}{E_1 A_1} + \frac{l}{E_2 A_2}} \tag{3.26}$$

Now if γ is made dependent on the model using the following relations, $\gamma_1 = \beta\left(\frac{E_1 A_1}{l}\right)$

and $\gamma_2 = \beta\left(\frac{E_2 A_2}{l}\right)$, we get, $\frac{u_4^{penalty}}{u_4^{lagrange}} = 1 + \frac{1}{\beta}$. As we see, for a high value of β the solution approaches that given by the Lagrange multiplier method.

3.3 Interface Element to model Delamination

The above-described Interface element can be used to model delamination. One feature of the interface element that facilitates delamination is the ability to release desired portion of the interface element smaller than the finite element itself. The general model based on which it is developed is the bilinear-softening model (Figure 3.2). Here the stresses increase to the strength of the material, so that it is proportional to the penalty parameter. Then the stiffness of the interface is reduced by decreasing the penalty parameter in the form, $\gamma = (1 - D)\gamma$, here D is a damage parameter and has a value between 0 and 1.

In ModeI delamination, the stress increases to strength of the material, until the relative displacement between the top and bottom finite element mesh is δ_0. Then the interface accumulates damage and when the relative displacement between the meshes is δ_f, the interface is completely debonded. As in the figure, when the relative displacements between the two FE meshes are between and δ_0 and δ_f, if there is unloading, it unloads to the origin. This is obtained by using , D, the damage parameter in the following manner

$$\sigma = (1 - D)\gamma\delta \tag{3.27}$$

37
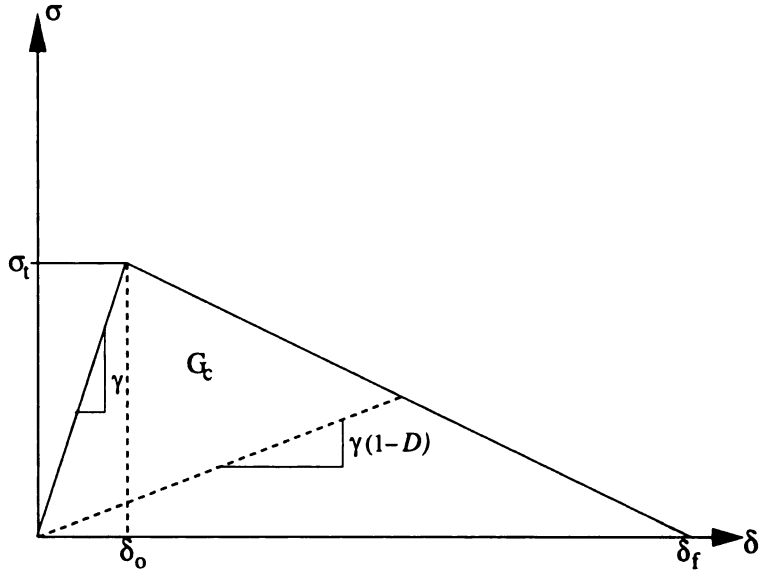
Figure 3.2: Bilinear Model

The value of D is computed from geometry as

$$D(\delta) = \frac{\delta_f(\delta - \delta_0)}{\delta(\delta_f - \delta_0)} \qquad (3.28)$$

Thus if one knows any two of the four interfacial properties, $G_c, \sigma_t, \delta_f, \delta_0$ the interface element can be described completely.

$$G_c = \frac{\delta_f \sigma_t}{2} \qquad (3.29)$$

$$\delta_0 = \frac{\sigma_t}{\gamma} \qquad (3.30)$$

Where, G_c is the strain energy release rate, σ_t is the ultimate strength of the interface, δ_0 is the relative displacement at the onset of failure and δ_f is the relative displacement when there is complete debonding of the surfaces. This bilinear interface model is applied to a sub-region of the interface element. This enables simulating delamination by releasing

38
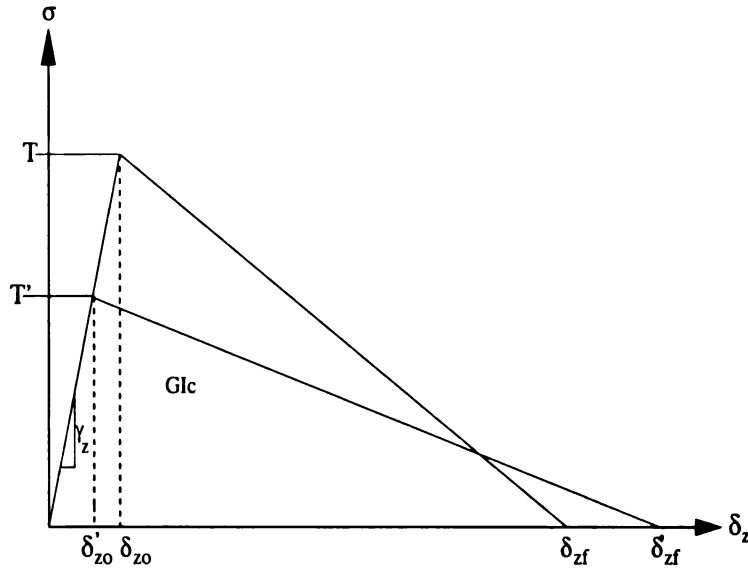
Figure 3.3: Updating tensile stresses

the desired portions of the interface element.

In general during an axial crush of a tube both Mode I and Mode II delamination are seen to take place. In order to simulate this , a quadratic failure criterion is used as follows.

$$\left(\frac{\sigma_z}{T}\right)^2 + \left(\frac{\tau_{xz}}{S}\right)^2 = 1 \tag{3.31}$$

$$\left(\frac{\delta_z}{\delta_{z0}}\right)^2 + \left(\frac{\delta_x}{\delta_{x0}}\right)^2 = 1 \tag{3.32}$$

Where, $\delta_{z0} = \frac{T}{\gamma_z}, \delta_{x0} = \frac{S}{\gamma_x}, \sigma_z = \gamma_z \delta_z, \tau_{xz} = \gamma_x \delta_x$

Based on this criterion updated values of T and S are calculated. Thus the interlayer strengths and the relative displacements at which they occur are updated for the mixed mode failure. Figures 3.3 and 3.4 illustrate this.

39
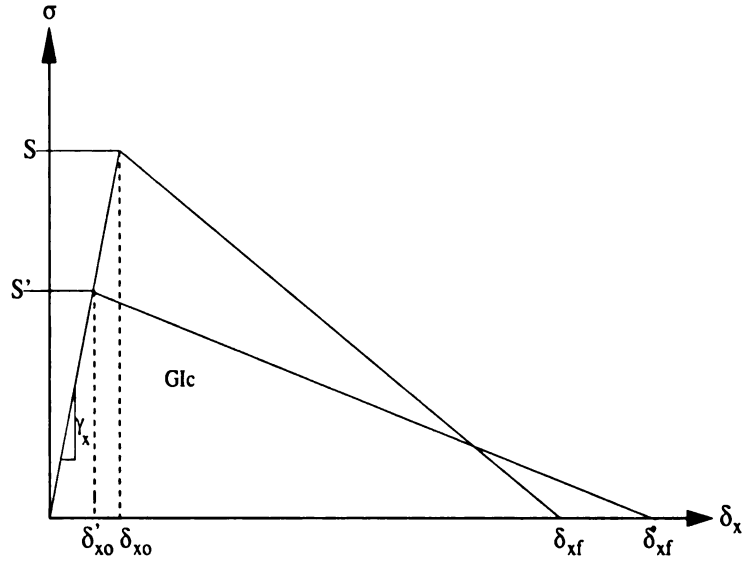
Figure 3.4: Updating shear stresses

Thus,

$$T' = \gamma_z \delta'_{z0} \tag{3.33}$$

$$S' = \gamma_x \delta'_{x0} \tag{3.34}$$

Similarly the quadratic failure criterion,

$$\left(\frac{G_1}{G_{1c}}\right)^2 + \left(\frac{G_2}{G_{2c}}\right)^2 = 1 \tag{3.35}$$

is assumed for the strain energy release rates and the values of G_{1c} and G_{2c} is updated for the model.

As mentioned in the various literature reviews it is also important to model friction between the interfaces. This is taken care of by ABAQUS itself. The model is constructed
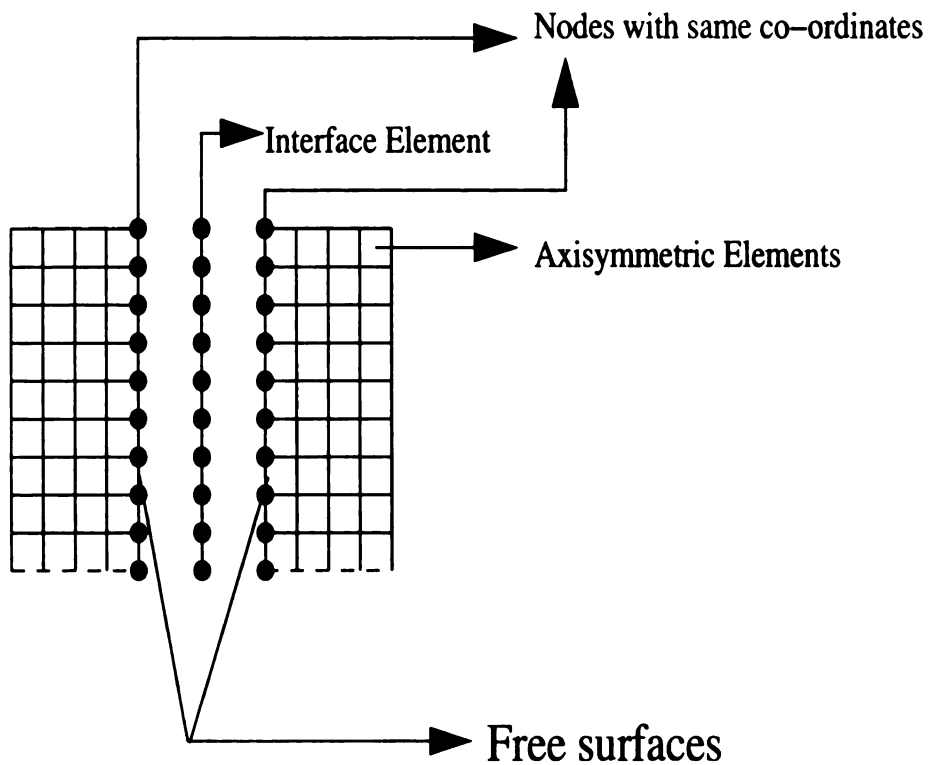
Figure 3.5: Interface Element enables to model friction between plies

in such a way that the layers of elements are joined by the interface elements. At the interface, the elements of one mesh are in reality not joined to the other, though the nodal co-ordinates are the same, they are nodes of different elements. In ABAQUS this allows us to model the two layers as contacting surfaces and hence include friction. This is illustrated in Figure 3.5.

3.3.1 Specification of the Interface Element for Input File

ABAQUS allows the specification of user element using the following keywords

- *USER ELEMENT

41

- *ELEMENT

- *UEL PROPERTY

The data card for the keywords their options and specification for the model is described below

*USER ELEMENT, NODE=12, TYPE=U1, PROPERTIES=10, IPROPERTIES=6,COORDINATES=2, VARIABLES=4

1, 2

This keyword specifies the use of a user element that is a FORTRAN program written for ABAQUS/STANDARD.

Options

- NODE=12: Specifies the total number of nodes that form a single interface element. This is actually the summation of N, M, NPS values of the UEL PROPERTY keyword. This may vary from one interface element to another but must be unique for a particular TYPE of interface element.

- TYPE=U1: Specifies the type of the interface element. Each type may have a unique property definition. Subsequent types may be given names as U2, U3 and so on. If all the interface elements on the interface have the same property, as is the case with the analysis performed for this work, they all may be of TYPE=U1.

- PROPERTIES=10: This specifies total number of properties that are required for the interface element. The default of 10 must be used.

- IPROPERTIES=6: This indicates the total number of integer properties required. This is a default value for the program and must not be changed.

- COORDINATES=2: Total number of coordinates for a node of an interface element. Since this is a 2D interface element it has a value 2. This is a default and cannot be changed.

- VARIABLES=4: Total number of solution dependent state variables that needs to be stored by the program. This is also a default value and must not be changed.

- *DATA CARD*: The data card 1, 2 indicates that two degrees of freedom are active for the nodes of the interface element.

*ELEMENT, TYPE=U1, ELSET=INTFACE1

3000,423,424,425,426,15001,15002,15003,15004,634,635,636,637

3001,426,427,428,429,15004,15005,15006,15007,637,638,639,640

3002,429,430,431,..

This keyword specifies the interface element number and the node numbers (already defined) which form the interface, (basically the connectivity for the interface elements).

All the elements with a unique property may be assigned to an element set INTFACE1 (ELSET=INTFACE1)

- *DATA CARD* In the example illustrated 3000,3001 are interface element numbers. 423 through 426 are nodes on the left mesh from top to bottom of interface element 3000. 15001 through 15004 are nodes that form the interface element 3000. They must be at least four in number and correspond to the value of NPS in the UEL PROPERTY definition. 634 through 637 are nodes that form the nodes of the right hand side mesh, from top to bottom. The specification for interface element 3001 is now straightforward from the explanation and Figure 3.6. It must be noted that the interface element nodes must coincide with finite element nodes at least at the ends, the intermediate nodes may not. However for the sake of simplicity in this case the nodes of the finite elements and interface elements coincide as indicated by Figure 3.6.

*UEL PROPERTY, ELSET=INTFACE1

```
**BETA,      THK1,        THK2,        E1,   E2,   Sr1,   GIc,   Sr2
 0.6670,   0.191112505, 0.191112505,25E+9,25E+9,20E+6,134.,23E+6
**GIIc,    FRICTION, N, M, ND, NEP, NPS, IFDAMG
 154.1,      0.0,    4, 4,  9,  5,   4,    1
```

The keyword specifies that the property described in the data card for this keyword is applicable for the element set INTFACE1
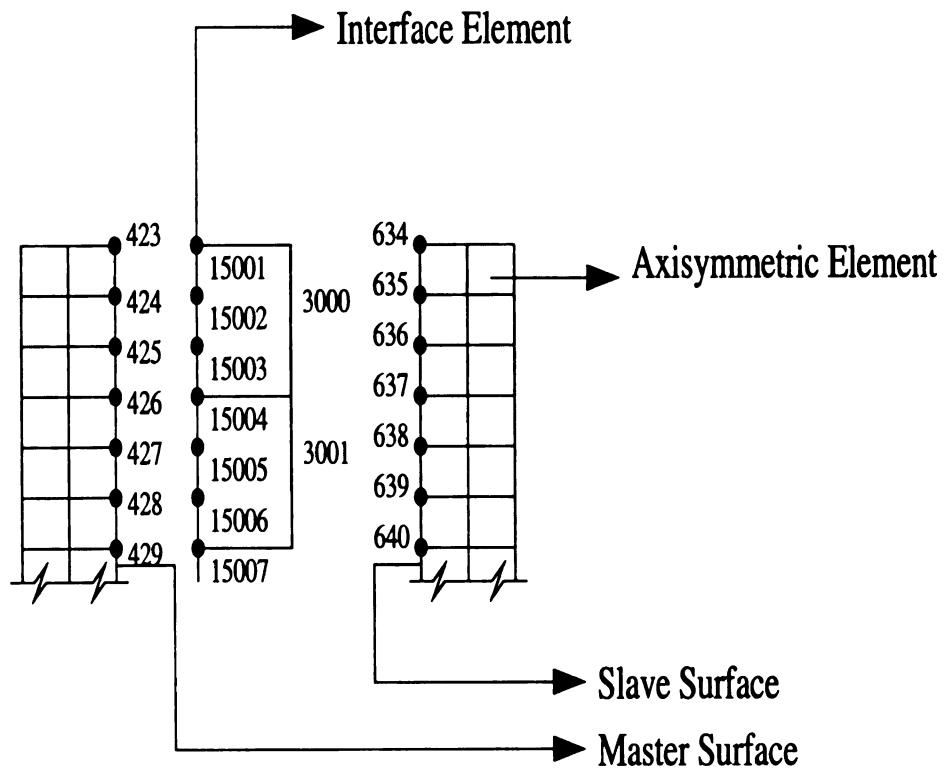
Figure 3.6: Specification Of Interface element nodes

<u>*DATA CARD:*</u> The specification of values for this datacard is most crucial for the analysis and is explained in sufficient detail in the following paragraphs.

- *BETA,* (β)

    Based on the explanation given on delamination implementation and the formulation of the interface element, it should be clear that the value of Beta (β) is related to the penalty parameter. The value of β specified here will be used in the code to enforce the constraint.

    The derivation to specify β value for the analysis is as follows. The Lagrange multiplier can be related to the penalty parameter in the following manner.

$$\lambda = \gamma C(u_1, u_2) \tag{3.36}$$

,where $C(u_1 u_2)$ is the constraint.

The Lagrange multiplier can be physically understood to be the force that is required to enforce the constraint.

Hence we have, (Figure 3.7)

$$F = \gamma \int_0^{dl} (V - u) dl \tag{3.37}$$

V is the primary degree of freedom for the interface element and u for the finite element nodes. Now, if we assume that the crack propagates a length of dl for a crack opening displacement of δ_0 at the maximum stress σ_u, then
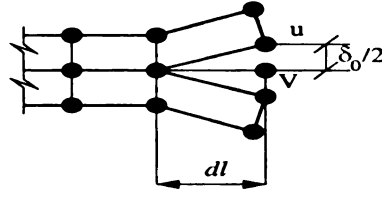
Figure 3.7: Illustration for derivation of γ

$$F = \frac{\gamma}{2}\delta_0 dl \tag{3.38}$$

, dividing both sides by the area, we get,

$$\gamma = \frac{(2)(\sigma_u)(thk)}{\delta_0} \tag{3.39}$$

The penalty parameter, γ, is related to beta (β) through the geometry of the structure as follows.

$$\gamma = \beta\left(\frac{(E)(thk)}{d}\right) \tag{3.40}$$

E ,The Young's modulus

d ,The length of a finite element along the interface

thk, Thickness of finite element mesh.

Equating the two values of γ, we get

$$\beta = \frac{2\sigma_u d}{E\delta_0} \tag{3.41}$$

Hence with appropriate values of σ_u, d, E, δ_0 (material/model dependent) one can specify the value of β required for the analysis. Since delamination is modeled for

47

both ModeI and ModeII any one of the values may be used to define the value of β. In using axisymmetric elements the thickness value may be specified as the circumference of a circle with radius at the interface element.

Ambiguity in γ definition

From the Figures 3.2, 3.3 and 3.4 the values of γ is given by:

$$\gamma = \frac{T}{\delta_0} = \gamma_1 \tag{3.42}$$

Essentially the slope of the stress/relative displacement graph. But in this section we have derived the relation,

$$\gamma = \frac{(2)(\sigma_u(or)T)(thk)}{\delta_0} = \gamma_2 \tag{3.43}$$

Clearly,

$$\gamma_2 = (2)(thk)\gamma_1 = (constant)\gamma_1 \tag{3.44}$$

Also, γ is just a large number that enforces the constraint, so the specification of γ is consistent as long as it's definition is made clear. So we can assume that the slope of the Stress/displacement is $\frac{\gamma_2}{constant} = \gamma_1$.

- $THK1$ and $THK2$

  These are the thickness of the left and right hand finite element meshes and have a value $2\pi r$, where r is the radius to the location of the interface element in the model.

- $E1$ and $E2$

  These are the Young's modulus of the left and right hand side meshes. For this analysis these values are the same.

48

- *Sr*1, GI_c

  These are the ultimate tensile stresses and critical strain energy release rates for Mode I delamination.

- *Sr*2, GII_c

  These are the ultimate shear stresses and critical strain energy release rates for Mode II delamination.

- Friction

  This specifies the coefficient of friction between the two surfaces. Since the code is successful in modeling contact between the two surfaces only for cases of small sliding, this is not used in the current analysis and a value of 0.0 is given. Instead the two meshes are modeled separately and contact is established by ABAQUS directly.

- N

  Number of nodes on the left hand mesh

- M

  Number of nodes on the right hand mesh

- NEP

  Number of evaluation points, Must be five and is a default

- NPS

  Total number of nodes forming an interface element. This must have a minimum

value of four.

- ND

  Specifies the number of subdivisions in an interface element. This must have a value greater than one. Greater the number of subdivision more accurately is the delamination predicted but more expensive is the solution. This enables releasing portions of the interface smaller than the finite element itself.

- IFDAMG

  Giving a value of 1 enforces the constraints and includes friction, a value of 0 simply prevents overlapping of the two meshes.

CHAPTER 4

Analysis

In this chapter, details of the Finite Element Analysis are described. Results of a few experiments that help to intuitively understand the effect of various parameters that affect the energy absorbed during the crush experiment are also discussed.

4.1 The Model

The Finite Element Model was based on simple axisymmetric (CAX4) elements and the initiator was modeled as an analytical rigid surface. Figure 4.1 illustrates the model. All nodes at the top of the tube were encastered (*fixed in all degrees of freedom*) while the initiator was given a displacement in the upward (or) 2 direction. Tube of length of 4 inches, outer diameter and a thickness of 2.5 inches and 0.075 inches respectively was chosen for the study.

As specified in section 3.3 the interface elements naturally allow us to model friction between the plies once delamination has taken place. *Due to severe contact convergence problems only two plies were used here to simulate delamination.*
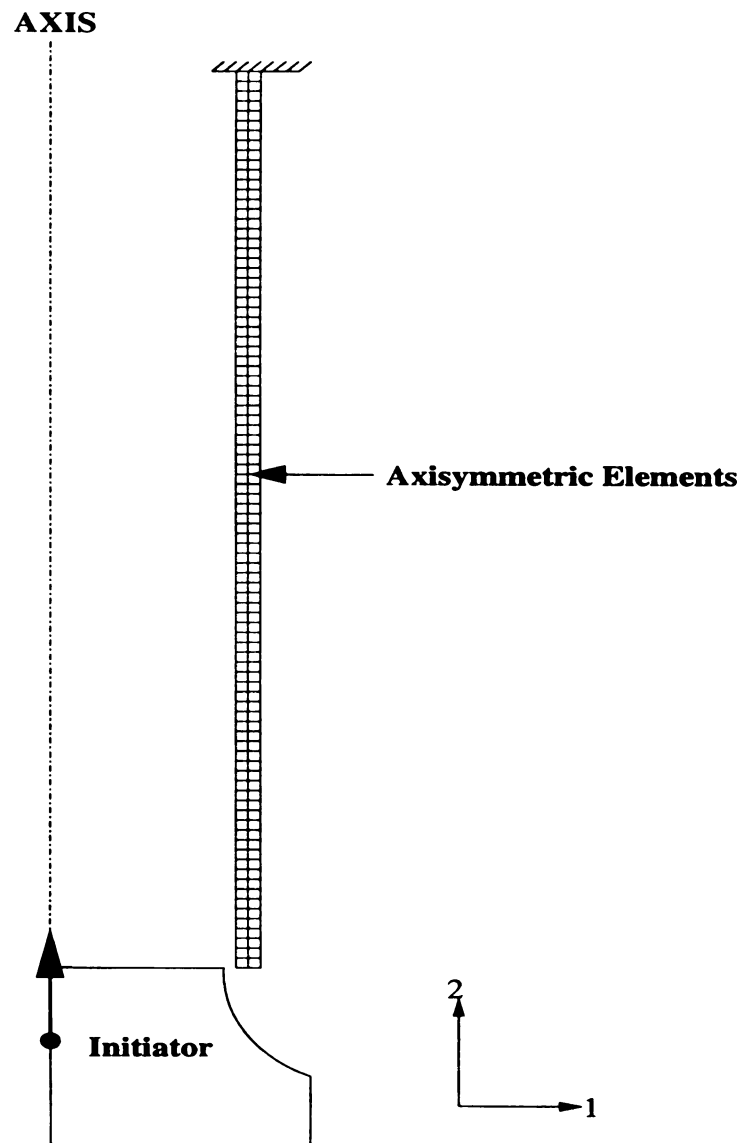
Figure 4.1: The Model

4.2 Concrete Material Properties

The following properties were chosen for simulating material failure in the concrete material model.

E, Young's Modulus	$2E + 10 \; \frac{N}{m^2}$
μ, Poisson's ratio	0.3
Strain ratio, see section 2.1.4, Page 27	1.2 or 2.4
Ultimate Tensile stress, σ_u	$155E + 6\frac{N}{m^2}$
Ultimate Compressive stress, σ_{uc}	$155E + 6\frac{N}{m^2}$

A visco–plastic parameter of $1E - 4$ was used to facilitate numerical convergence, avoid mesh-dependency and prevent strain localization. Please see [17, 18, 21–23] for details.

4.3 Interface Element Properties

The interface element required to simulate delamination was given the following properties as in Table 4.1. (Section 3.3.1, Page 41)

It can be noted that two values are given for ModeII interface strength and four values of strain energy release rates are specified. These values are used to see the effect of delamination on the energy absorbed. This method of specification of the factors enables automatic ANOVA studies using softwares. Detailed explanation of these factors are given in the following section.

Beta, β	0.967619047
THK1,THK2	$0.193506399m$
E1,E2	$2.0E + 10\frac{N}{m^2}$
Sr1	$80E + 6\frac{N}{m^2}$
GI_c	$352\frac{N}{m}$
Sr2	$20E + 6\frac{N}{m^2}$ (or) $20E + 7\frac{N}{m^2}$
GII_c	$50\frac{N}{m}$ (or) $100\frac{N}{m}$ (or) $5000\frac{N}{m}$ (or) $10000\frac{N}{m}$
FRICTION	0.0
N	4
M	4
ND	6
NEP	5
NPS	4
IFDAMG	1

Table 4.1: Interface Properties

4.4 Factors and Their Levels

For preliminary analysis the following factors were considered.

1. Radius of the initiator ($\frac{3}{16}$ inch and $\frac{5}{16}$ inch)

2. Friction between the initiator and the tube (0.0 and 0.3)

3. Material Strain Ratio (1.2 and 2.4)

4. Strength of the interface ($20E + 6\frac{N}{m^2}$ and $20E + 7\frac{N}{m^2}$)

5. Relative Displacement Ratio (5 and 10)

6. Friction between the plies (0.0 and 0.2)

Each factor has 2 levels and this amounts to performing 2^6 or 64 experiments to perform the analysis of variance. The contribution of a certain factor, in percentage is obtained

by taking the ratio of sum of squares for that factor to the total sum of squares [26]. The next chapter deals with the details of the procedure to perform the ANOVA and obtain the contributions.

The first two factors can be considered as *model related factors*, the third is *material dependent factor* while the last three are related to *delamination*. The model and the friction factors are very direct and are available in the ABAQUS input file to be changed directly. The specification of other factors are explained below.

4.4.1 Material Strain Ratio

This factor is considered to study the sensitivity of the response to the *material strain energy release rates*. Please see Figure 4.2. From section 2.1.4, page 27 we see that the strain energy release rate depends on the strain ratio through the expression

$$G_c = \frac{1}{2}\sigma_u(l)(SR)\varepsilon_f \tag{4.1}$$

Therefore for a certain ε_f, σ_u and l, each value of SR we will have a different strain energy release rate value. Please see section 2.1.3, page 21 to implement this factor.)

In general it is observed that higher values of negative slope in the post failure region of material models cause serious convergence problems. If the ANOVA study indicates that the response is significantly sensitive to the strain energy release rate (Area under the stress vs crack opening displacement diagram) then it would be possible to maintain the
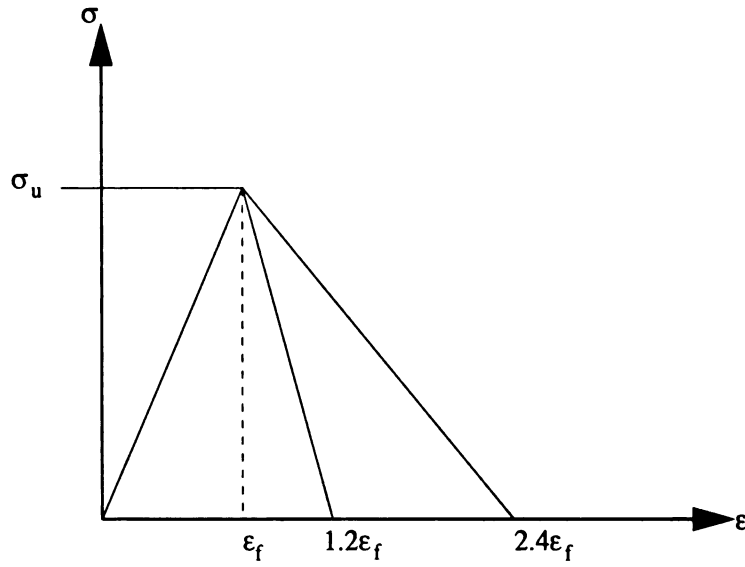
Figure 4.2: Illustration of Strain Ratio Factor

strain energy release rate while lowering the value of the negative slope to obtain quicker numerical results. Figure 4.3 illustrates this.

4.4.2 Strength Of the Interface

This factor has two levels with each level depicting the ModeII strength. The lower strength causes delamination while the higher one does not. By including this as a factor, the effect of delamination on the total energy absorbed can be studied. This method of implementing this factor enables automation of the ANOVA study using softwares.

Experiments where delamination is not required to take place may also be run by modifying the input file to not include the interface element. This will save sufficient computation time and is used in the current work.

$$\frac{1}{2}\sigma_{u1}u_{01} = \frac{1}{2}\sigma_{u2}u_{02} = G_c$$
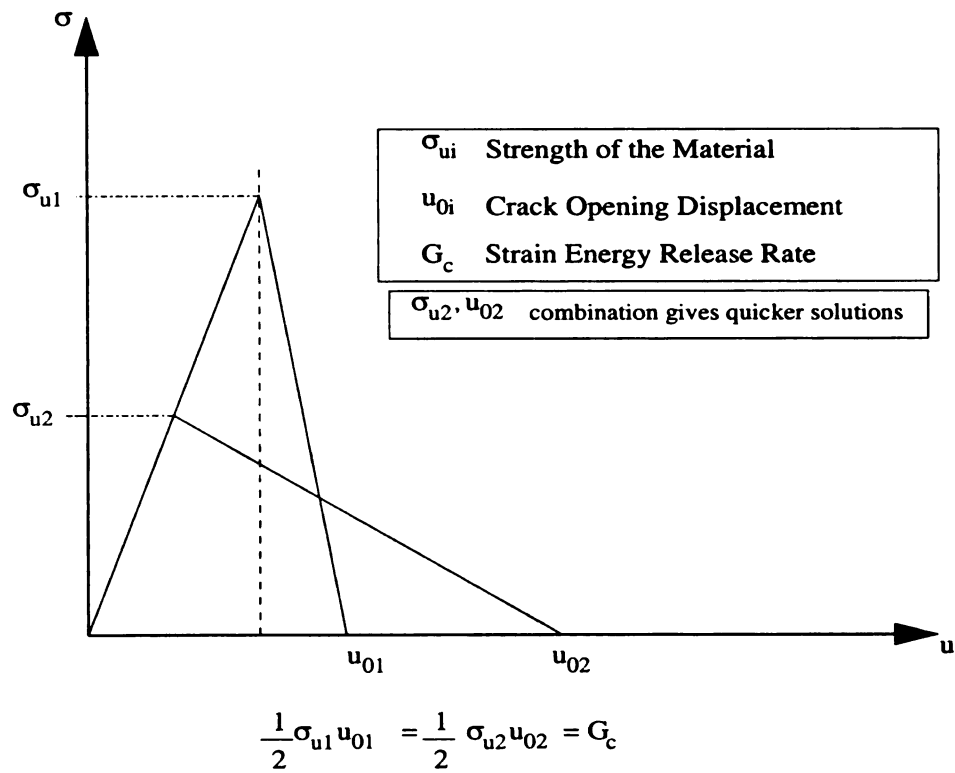
Figure 4.3: Purpose of Strain Ratio Factor
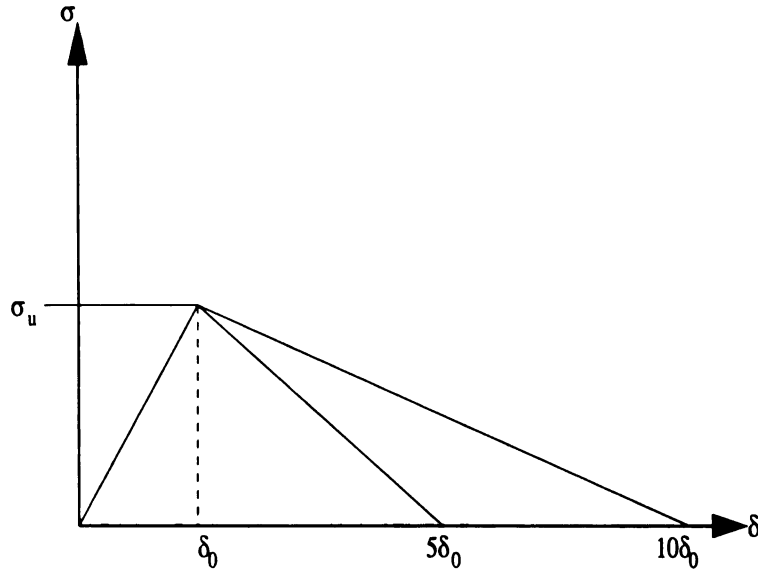
Figure 4.4: Illustration Of Relative Displacement Ratio factor

4.4.3 Relative Displacement Ratio (RDR)

The purpose of this factor is to study the effect of ModeII strain energy release rate on the total energy absorbed. The values of the **Relative Displacement Ratio** refers to the ratio of the displacement between the layers at failure to the displacement at complete loss of interface strength $(\frac{\delta_f}{\delta_0})$ (Figure 4.4). In ModeII these refer to the sliding displacement. The following expressions together with Figure 4.5 illustrate this factor

$$GII_c = \frac{1}{2}(\sigma_u)\delta_f \tag{4.2}$$

$$GII_c = \frac{1}{2}(\sigma_u)(RDR)\delta_0 \tag{4.3}$$

It is expected that the conclusions from ANOVA for this effect will be helpful in the same sense as the Strain Ratio factor. The RDR factor is also implemented by changing the

58
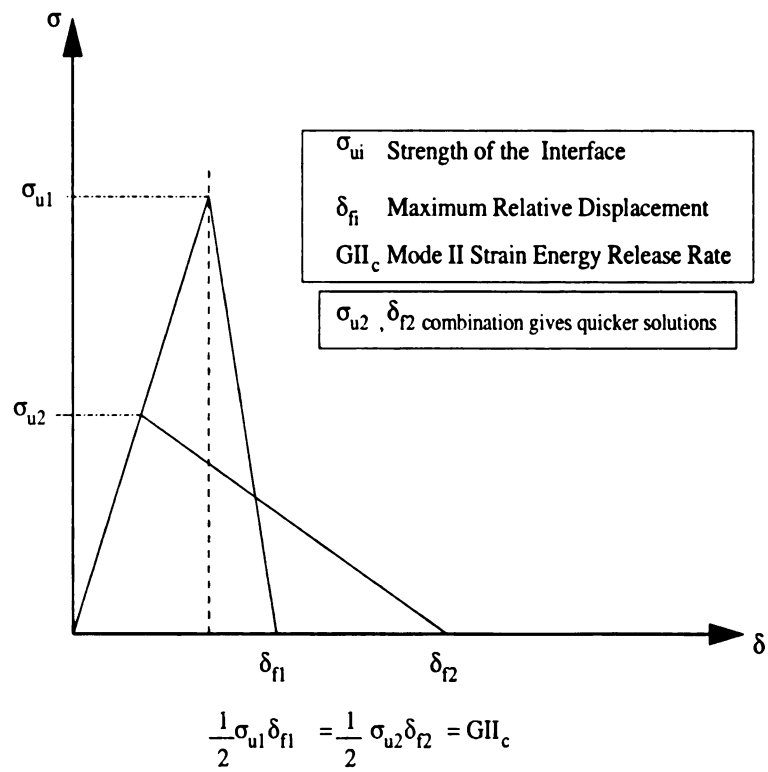
Figure 4.5: Purpose of Relative Displacement Ratio Factor

59

value of the Strain Energy release rate in the *UEL PROPERTY keyword. The strain energy release rate is dependent on the ModeII strength and the RDR value. The δ_0 term can be eliminated using a constant value for the penalty parameter. The following calculations clarify this and are useful when using a software to automate the ANOVA study done for this work.

We know from section 3.3.1, equation 3.39

$$\gamma = \frac{(2)(THK)(\sigma_u)}{\delta_0} \tag{4.4}$$

$$\frac{\sigma_u}{\delta_0} = \frac{\gamma}{(2)(THK)} \tag{4.5}$$

and from equation 3.41,

$$\beta = \frac{(2)(\sigma_u)(d)}{(E)(\delta_0)} = \frac{(\gamma)(d)}{(E)(THK)} = CONSTANT \tag{4.6}$$

Therefore β will be a constant for all the analysis.

Now from equation 4.3

$$GII_c = \frac{1}{2}(\sigma_u)(RDR)\delta_0 \tag{4.7}$$

(or)

$$GII_c = \frac{(\sigma_u^2)(RDR)(THK)}{\gamma} \tag{4.8}$$

In this way, while automating ANOVA studies, the GII_c values can be made as a variable, dependent on RDR and σ_u factors.

4.5 Calculations

In this section all the required calculations are shown to facilitate rerunning of analysis for future research.

4.5.1 Calculation of β

From the previous sections we know β is a constant for all the analysis that will be performed for the ANOVA study.

$$\beta = \frac{(\gamma)(d = \frac{L}{N_e})}{(E)(THK)} \qquad (4.9)$$

Where,

d, is the length of a finite element along the interface

L, is the Length of the tube in meters ($4'' = 0.1016m$)

N_e, is the number of elements along the length of the tube (210 for model used)

$$\gamma = \frac{(2)(THK)(\sigma_u)}{\delta_0} = \frac{2*0.193506399*2E+7}{1E-6} = 7.74025596E+12 \qquad (4.10)$$

$$\beta = \frac{7.74025596E+12 * \frac{0.1016}{210}}{2E+10*0.193506399} = 0.967619047 \qquad (4.11)$$

4.5.2 Calculation of Material Strain Energy Release Rates

We know that,

$$G_{c,SR} = \frac{1}{2}\sigma_u(\varepsilon_f)(SR)(l) \qquad (4.12)$$

$$\frac{\sigma_u^2(SR)(l)}{2E} = \frac{2.4025E+16*(1.2)*4.808E-4}{2*2E+10} = 346.5366 \qquad (4.13)$$

$$\frac{\sigma_u^2(SR)(l)}{2E} = \frac{2.4025E+16*(2.4)*4.808E-4}{2*2E+10} = 693.0732 \qquad (4.14)$$

61

4.5.3 Calculation of Mode II Strain Energy Release Rates

From section 4.4.3

$$GII_{c,\sigma_u,RDR} = \frac{(\sigma_u^2)(RDR)(THK)}{\gamma} \tag{4.15}$$

$$GII_{c,2E+7,5} = \frac{4E+14*5*0.193506399}{7.74025596E+12} = 50 \tag{4.16}$$

$$GII_{c,2E+7,10} = \frac{4E+14*10*0.193506399}{7.74025596E+12} = 100 \tag{4.17}$$

The following calculations are required only if analysis requiring no delamination are performed with a high value for the interface strength (useful while automating ANOVA through softwares). Analysis where no delamination is required can be easily and efficiently run by modifying the input file to not include the interface element.

$$GII_{c,2E+8,5} = \frac{4E+16*5*0.193506399}{7.74025596E+12} = 5000 \tag{4.18}$$

$$GII_{c,2E+8,10} = \frac{4E+16*10*0.193506399}{7.74025596E+12} = 10000 \tag{4.19}$$

4.6 Preliminary Analysis

As indicated previously, due to a high degree of non-linearities, convergence was a serious problem with all the analysis in this work. All the analyses did not run to completion due to these non-linearities. Several analysis were performed to determine the robustness of the finite element software to various values of these factors. Two such experiments that enabled to determine final values of one factor and also helped in deciding the the total final initiator displacement are discussed below.

4.6.1 EXPERIMENT 1

In this experiment two tubes of same dimensions were crushed using two initiators of different radii ($\frac{3}{16}$ *inch* and $\frac{5}{16}$ *inch*). The initiators were forced to cover a distance of 1.5 inches. Other properties used for this experiment are tabulated in Table 4.2

No delamination element was used for this experiment. The Energy absorbed for higher radiussed and lower radiussed initiator was 319.38*J* and 192.32*J* respectively. This indicates that the lower radiussed initiator increases the energy absorbed.The peak load is also higher for the lower radiussed initiator. Please see Figure 4.6 and Figure 4.7 and Table 4.3

From the above results it can also be observed that the contribution of friction is approximately the same for both the experiments. This concludes that the interaction between the radius effects and friction effects are negligible.

The time required for the analysis using the $\frac{3}{16}$ inch radius initiator was as long as 2 days and around 20,000 increments was needed. It hence was agreed that a $\frac{5}{16}$ inch radius initiator would be used for all the analysis in the ANOVA study.

E,Young's Modulus	$2E+10\ \frac{N}{m^2}$
μ,Poisson's ratio	0.3
Strain ratio	1.2
Ultimate failure stress,σ_u	$155E+6\frac{N}{m^2}$
Friction coefficient	0.3

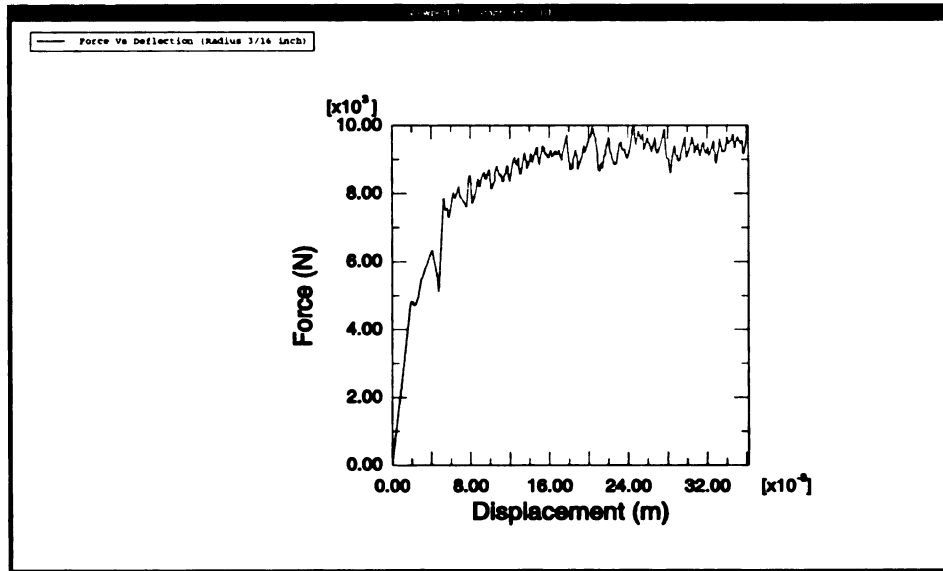Table 4.2: Values used for Experiment 1

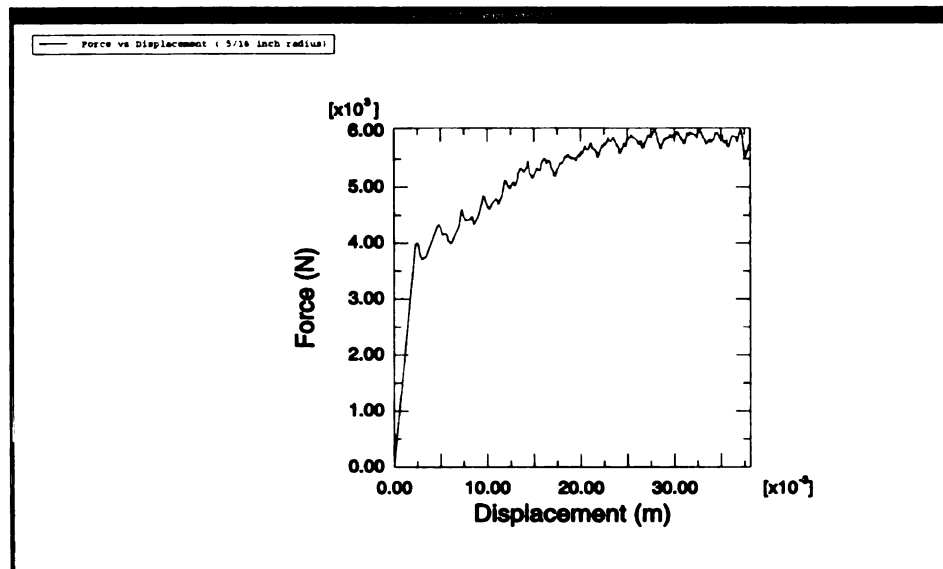Figure 4.6: Force vs Deflection with $\frac{3}{16}$ inch radiussed initiator

Figure 4.7: Force vs Deflection with $\frac{5}{16}$ inch radiussed initiator

Usual features of a typical force deflection diagram can be noticed in Figure 4.7. It can be divided into three main zones.

Zone I: In this region there is a steady increase in the load as the tube is deformed. This indicates that the tube is deforming elastically. The first drop in the load around $4KN$ corresponds to the beginning of material failure.

Zone II: This zone indicates a steady increase in the load along with failure taking place in the tube. The zone directly leads into the sustained crushing zone (ZONE III).

Zone III: In this zone sustained crushing is seen to be taking place, where the load oscillates about a mean crushing load indicating progressive failure of the tube.

4.6.2   EXPERIMENT 2

In one of the experiments the $\frac{5}{16}$ inch radius initiator was used and delamination was allowed to take place with an interface strength of $2E + 7\frac{N}{m^2}$, a strain ratio of 2.4 was used in this case. No friction was used, between the plies and between the tube and initiator. This analysis died with the displacement of the initiator being only 0.69375 inches. This was the analysis with the lowest value for the final initiator displacement. After careful inspection of the deformed configuration (Figure 4.8) and the ABAQUS message file it was concluded that contact between the plies caused severe convergence problems. *Since*

Radius	Total Energy Absorbed	Energy Absorbed due to Frictional Effects	Percentage contribution of friction
$\frac{3}{16}inch$	319.38J	145J	45.4
$\frac{5}{16}inch$	192.32J	92.2J	47.7

Table 4.3: Results for Experiment 1
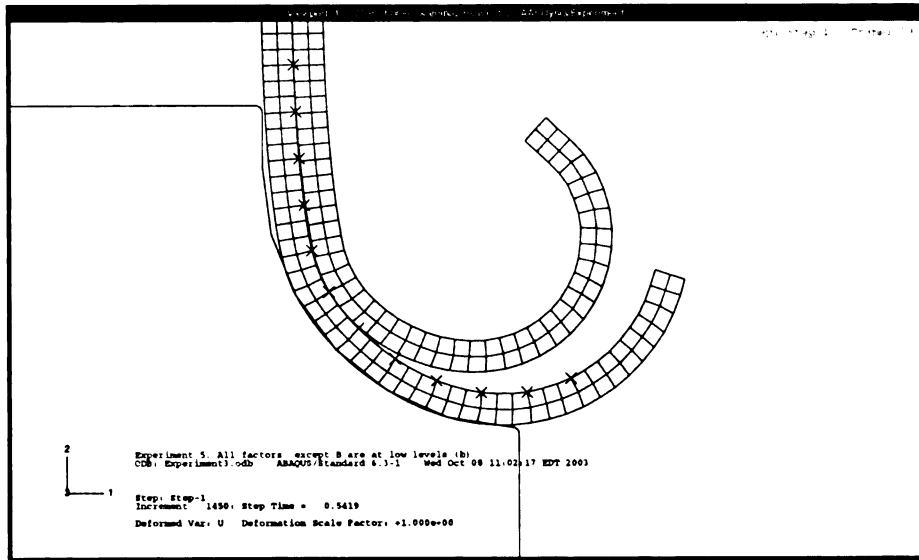
Figure 4.8: Illustrating delamination

the delamination code used in this work does not have the capability to write required data into a restart file, analysis involving delamination could not be restarted if they died due to problems in numerical convergence. It is however true that responses used for ANOVA must be for a certain final initiator displacement. It was therefore agreed that response up to 0.69375 inches of initiator displacement would be used for the ANOVA study.

CHAPTER 5

Analysis of Variance

5.1 ANOVA

Analysis of variance (ANOVA) is a well known method in the field of design and analysis of experiments. The use of ANOVA here, is to know which factors contribute significantly to the variability in the response. This is called **Factor Screening**. For sake of continuity a brief description on the procedure to perform ANOVA is described in this chapter. For details on ANOVA please see [26]. Finally results of ANOVA are tabulated and are described in detail. A section describing future extension of this work for automated analysis of variance is given with a motivation for incorporating "localization limiters" in material models for composite materials involving softening.

Let a *response* say *Energy absorbed*, during crushing of the tube be assumed to be dependent on five *factors* such as, *A, B, C, D, E*. These factors can be qualitative (*Presence/absence of delamination*) or quantitative (*numerical values*). Let each of these factors have only two *levels* each. This means that we want to study the response for 2 values of each of these factors. This will give us a total of $2 * 2 * 2 * 2 * 2 = 2^5 = 32$ experiments to be performed and are referred to as a **full factorial** study. Apart from each of the factors individually affecting the response (*Main Effect*), there may be interactions (*Interaction effect*) among these factors. If it is known in advance that interaction of certain factors do not affect the response, then a subset of the $2^5 = 32$ experiments could be performed and

this is called **fractional factorial** study.

If the experiments were performed in a laboratory with testing equipments, each of these experiments would be performed more than once in order to negate the effect of *random errors* that creep in due to several uncontrollable factors. However, performing experiments on a computer give rise to *deterministic* responses. Hence each of the 32 experiments need to be performed only once.

The basic idea of Analysis of variance stems from dividing the total variability into its component parts. The *total corrected sum of squares* (SS_T) is taken as a measure of variability. It is the *sum of squares of the differences between individual treatment values and the grand averages*. The total sum of squares is taken as the *sum of squares of the differences between treatment averages and the grand averages* ($SS_{Treatment}$) plus the *sum of the squares of the differences of observations within treatments from the treatment average* (SS_E). Clearly $SS_{Treatment}$ is a measure of differences between treatment means, while SS_E can be only due to random error. Since computer experiments are deterministic, this term vanishes. So we have:

$$SS_T = SS_{Treatment} \qquad (5.1)$$

The $SS_T = SS_{Treatment}$ are equal to the *sum of squares due to each effect* (including *Main effect* and *interaction effects*). This gives:

$$SS_T = SS_{Treatment} = SS_A + SS_B + SS_C + SS_D + SS_E + SS_{AB} \cdots \cdots + SS_{ABCDE} \quad (5.2)$$

68

	B1								B2							
	C1				C2				C1				C2			
	D1		D2		D1		D2		D1		D2		D1		D2	
	E1	E2	E1	E2	E1	E2	E1	E2	E1	E2	E1	E2	E1	E2	E1	E2
A1	*(1)*	*e*	*d*	*de*	*c*	*ce*	*cd*	*cde*	*b*	*be*	*bd*	*bde*	*bc*	*bce*	*bcd*	*bcde*
A2	*a*	*ae*	*ad*	*ade*	*ac*	*ace*	*acd*	*acde*	*ab*	*abe*	*abd*	*abde*	*abc*	*abce*	*abcd*	*abcde*

1, 2 indicate low and higher levels of the factor

Figure 5.1: Labeling the responses

Here, $SS_A, SS_B, SS_C, SS_D, SS_E$ are the sum of squares of the main effects while SS_{AB}....
etc, are the sum of squares of the interaction effects. Thus the contribution of each effect to
the total variability is simply found by taking the ratio of the sum of squares for that effect
to the total sum of squares.

$$Contribution_{ABCE} = \frac{SS_{ABCE}}{SS_T}$$ (5.3)

Calculation of the sum of squares for each effect is done using *contrasts* for each effect
in the following manner.

Each response is labeled as *a, b, c, d, e, ab, ...abde,......abcde*. Please see Figure 5.1.
The presence of an alphabet indicates a higher level for that factor and absence of that

69

alphabet indicates a lower level of that factor. For example, *abce* indicates the response that was obtained for the experiment that used high levels of factor A, B, C, E and a low level of factor D. A simple method to calculate the *contrast* is given by,

$$Contrast_{ABCD} = (a-1)(b-1)(c-1)(d-1)(e+1) \tag{5.4}$$

$$= abcde + cde + bde + ade + bce + ace + abe + e + abcd + cd + bd + ad + bc + ac + ab + (1)$$

$$-a - b - c - abc - d - abd - acd - bcd - ae - be - ce - abce - de - abde - acde - bcde \tag{5.5}$$

Note: (1), indicates response, when all factors are at a low level

Once the contrasts are estimated, the effects and the sum of squares are estimated as follows:

$$S_{ABCD} = \frac{1}{2^4}(Contrast_{ABCD}) \tag{5.6}$$

$$SS_{ABCD} = \frac{1}{2^5}(Contrast_{ABCD})^2 \tag{5.7}$$

5.2 Results and Discussion

The various factors considered to study the sensitivity of the response are tabulated in Table 5.1. ANOVA was performed using method described in the previous sections.

Low values, of factor E is assumed, as higher values did not give satisfactory responses interms of final initiator displacement. The analysis failed to converge for higher values for this factor and restart was not possible due to reasons specified in section 4.6.2, Page 65. Even with the current values, each analysis completed to different extents. It was hence decided to use responses for only 0.69375 inches of the final initiator displacement (Experiment 2, previous chapter) for the ANOVA. Due to this reason the force deflection

Factor Label	Factor Description	Levels	Values
A	Friction between initiator and tube	2	0.0 and 0.3
B	Strain Ratio	2	1.2 and 2.4
C	Delamination	2	Presence and absence
D	Relative Displacement Ratio	2	5 and 10
E	Friction between plies	2	0.0 and 0.2

Table 5.1: Factors and their levels

diagrams shown henceforth may not show sustained crushing or (**ZONE III**). *It can also be noted that factors D and E have relevance only if delamination takes place, hence only 20 experiments need to be performed.*

The responses for each experiment and the contribution to the variability from each factor is given in Tables 5.2 and 5.3.

It is found that the contribution from the interaction effects to the total variability of the response are negligible. The *Main Effects* of factors **A, B, C** have significant contribution while the other factors have no contribution at all.

From Table 5.3 it is evident that about 61.97% of the variability in the response can be attributed to friction between the tube and the initiator, 10.39% to the strain ratio factor and 25.55% to delamination. It is observed that the presence of delamination decreases the total energy absorbed and and has a significant contribution to the variability in the response. It can be hence concluded that numerical modeling of delamination is crucial for accurate represention of the failure of composite tubes. In this work it was observed that

Experiment	Response(Joules)
(1)	25.67
a	48.79
b	35.54
ab	62.5
c	40.76
ac	74.21
bc	51.55
abc	88.2
d	26.5
ad	49.9
bd	36.2
abd	62.8
cd	40.76
acd	74.21
bcd	51.55
abcd	88.2
e	27.2
ae	50.1
be	39.7
abe	64.3
ce	40.76
ace	74.21
bce	51.55
abce	88.2
de	27.1
ade	51.1
bde	37.2
abde	65.8
cde	40.76
acde	74.21
bcde	51.55
abcde	88.2

Table 5.2: Response for Each Experiment

delamination takes place during the early stages of the crush thus decreasing the overall

stiffness of the tube causing low peak forces and hence low energy absorption. Figures 5.2

72

Factors	Contribution (%)
A	61.97
B	10.39
C	25.55
D	0
E	0.06
AB	0.18
AC	1.73
AD	0.01
AE	0
BC	0
BD	0
BE	0.01
CD	0
CE	0.06
DE	0
ABC	0
ACD	0.01
ADE	0.01
AEB	0
AEC	0
BCD	0
BDE	0
BEC	0
CDE	0
BDA	0
ABCD	0
ACDE	0.01
BCDE	0
CABE	0
DBAE	0
ABCDE	0

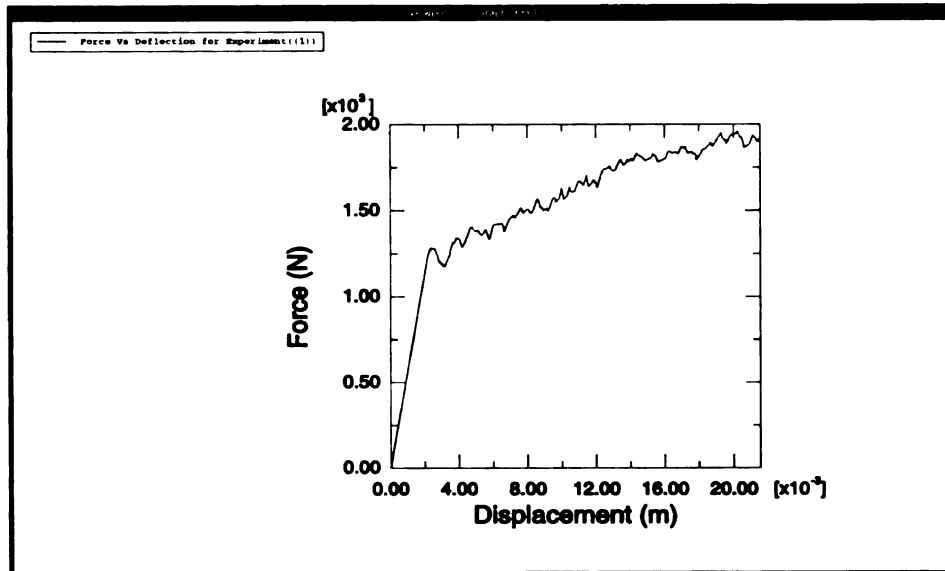Table 5.3: Contributions of each factor

and 5.3 illustrates this.

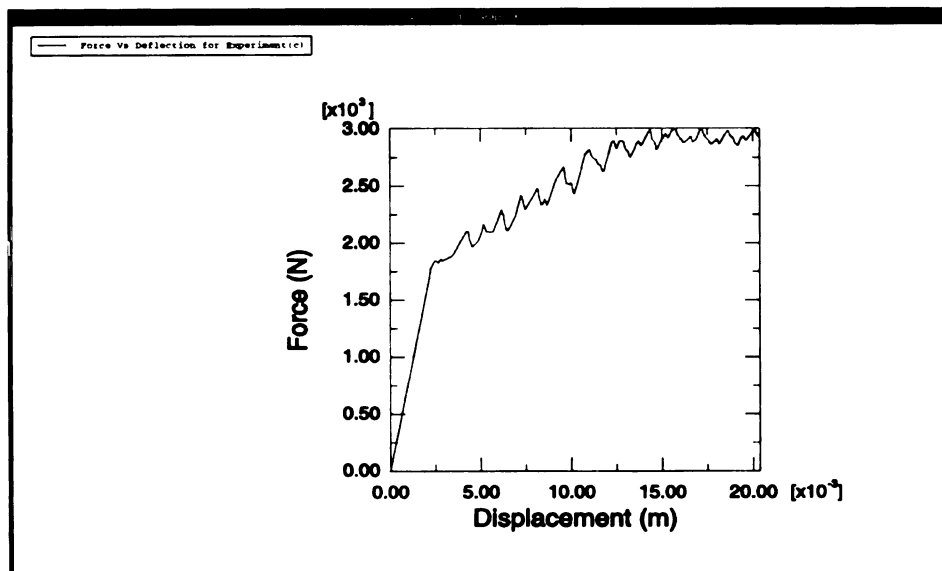Figure 5.2: Force vs Deflection for Experiment ((1))

Figure 5.3: Force vs Deflection for Experiment (c)

The friction factor (A) plays a vital role and positively increases the energy absorbed. This can be observed from Figures 5.4 and 5.5. Fiction between the plies factor (E) does not affect the response significantly and may be neglected in this case. However, it is important to increase the number of plies to know the effect of this factor in greater detail. Material strain energy release rate (factor B) describes about 10.39% of the variability
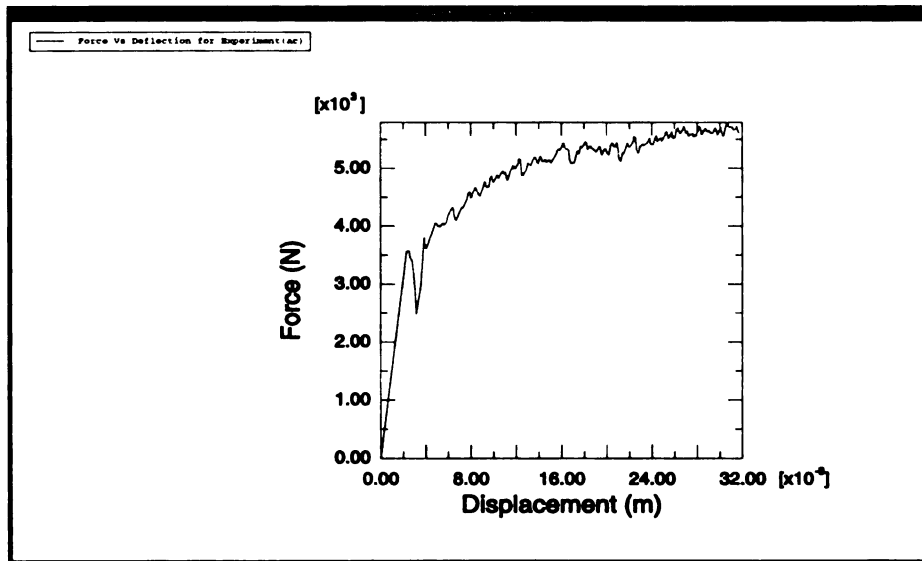

Figure 5.4: Force vs Deflection for Experiment(ac), *High friction coefficient*

in the response and plays a vital role. This suggest that a higher material strain energy release rates increases the energy absorbed by the tube during failure. The sensitivity of the response to this factor enables to improve the convergence of the analysis, as specified in section 4.4.1, Page 55. This phenomenon is demonstrated in the next section. Delamination strain energy release rate (D) does not affect the response at all and hence suggests that it can be neglected. However, it may be important to consider more plies for a more
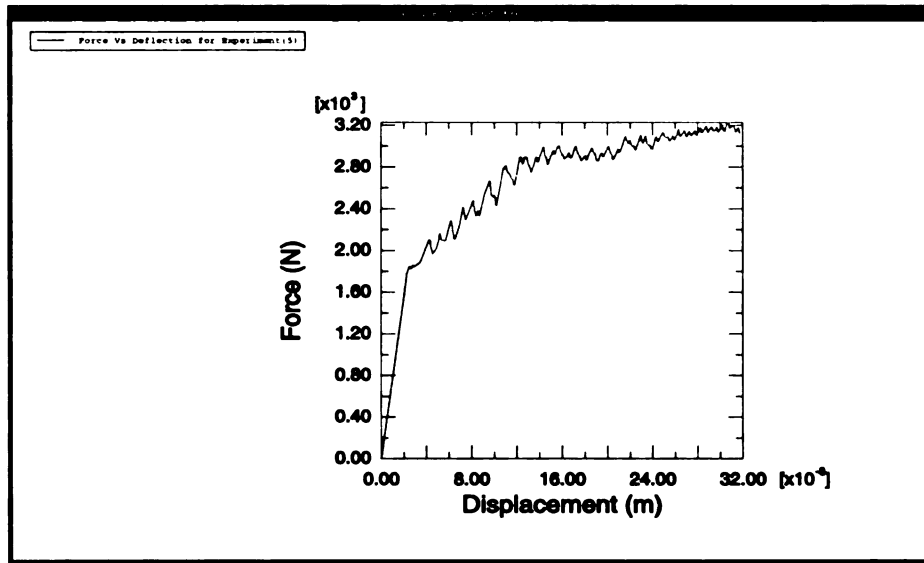
Figure 5.5: Force vs Deflection for Experiment (c), *Low friction coefficient*

convincing conclusion on this factor.

5.2.1 Effect of Strain Ratio

It was mentioned in 4.4.1, page 55 that decreasing the negative slope, in post failure region of the stress–strain diagram can cause improved convergence, if the ANOVA results indicate high sensitivity to the Strain Ratio factor. From Table 5.3 it can be seen that there is 10.39% of contribution through the strain ratio factor to the variability in the energy absorbed.

To verify the effect of strain ratio, three experiments were conducted. For all three experiments strain energy release rate of 346.5366 was considered. The strain at complete loss of strength was considered at three different strain ratios (1.2, 2.4 and 4.8). Please see
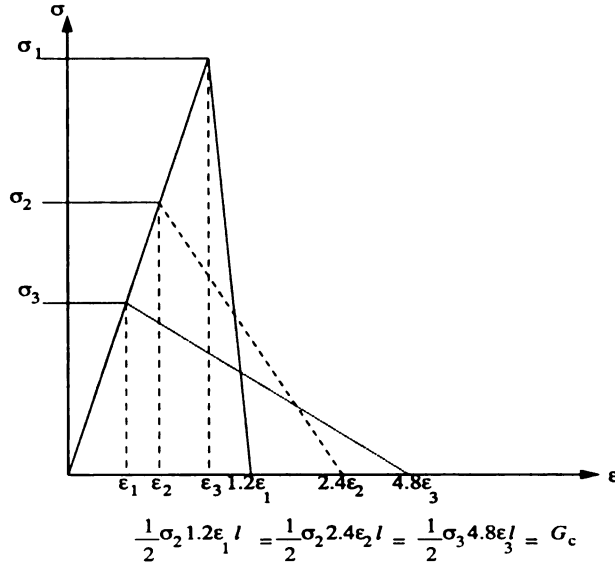
Figure 5.6.

Figure 5.6: Effect of Strain Ratio

For a constant strain energy release rate the modified strength was found using the following derivation.

$$G_c = \frac{1}{2}\sigma_f l(SR)\varepsilon_f \tag{5.8}$$

$$G_c = \frac{1}{2}\sigma_f l(SR)\frac{\sigma_f}{E} \tag{5.9}$$

$$\sigma_f = \sqrt{\frac{2G_c E}{l(SR)}} \tag{5.10}$$

For the three different strain ratios, the strengths, energy absorbed and number of increments required to complete the analysis for 1.25 inches of final initiator displacement are tabulated in Table 5.4. It is observed that maintaining the strain energy release rate while

77

lowering the negative slope in the post failure region improves convergence. An increase in the Strain Ratio by a factor of 2, improves convergence by nearly 50% (in terms of the number of increments) while the decrease in the energy absorbed is 13%. This indicates that a careful choice of the strain ratio, will help improve convergence without compromising on the results.

SR	Strength, in Pa	Response, (J)	No. of Increments	Time to complete
1.2	$155E + 6$	84	5833	7.7 Hrs
2.4	$109.601E + 6$	73	2837	2.5 Hrs
4.8	$77.5E + 6$	51	1998	1Hr 40 min

Table 5.4: Effect of Strain Ratio

Figures 5.7 through 5.12 show the deformed shapes and the force deflection diagram of all the three analyses. Large values of the strain ratio, cause strain localization as can be observed in Figure 5.9, at regularly spaced intervals. This strain localization manifests itself as huge drops in the load deflection diagram (Please see Figure 5.12). Such a behavior does not represent the response curve correctly and hence places a limit on the choice of the Strain Ratio value. The cause of this strain localization is attributed to the reduced viscoplastic effect. In other words, the introduction of rate dependency by viscoplastic regularization of the constitutive equations acts as "localization limiters". Quicker convergence due to high Strain Ratio negates the viscoplastic effects and causes strain localization. Please see [21–23] for further details.
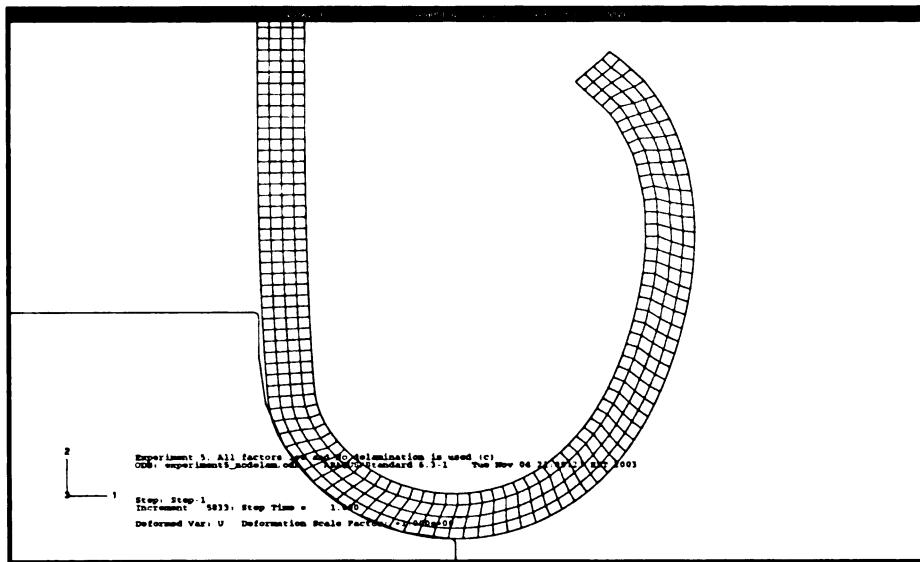
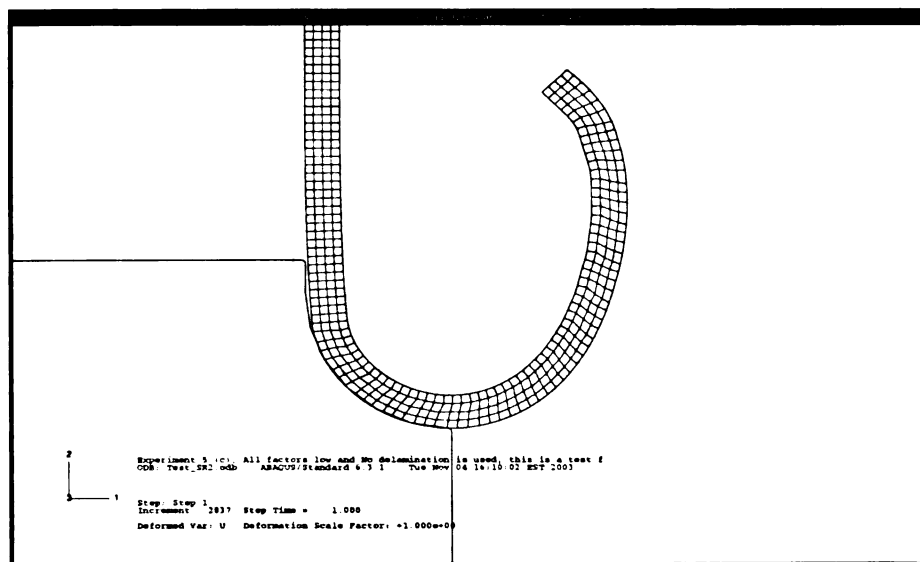Figure 5.7: Deformed shape , Strain Ratio = 1.2

Figure 5.8: Deformed shape, Strain Ratio = 2.4
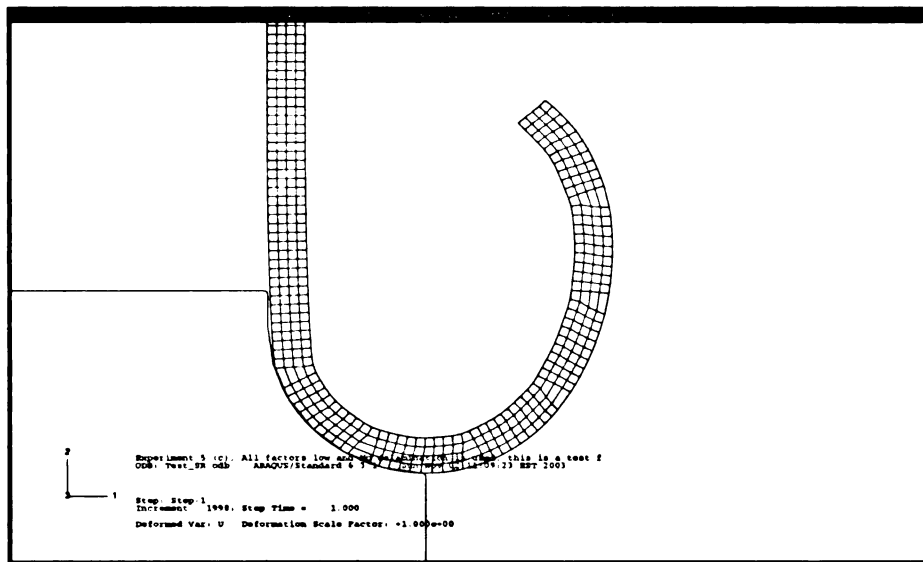
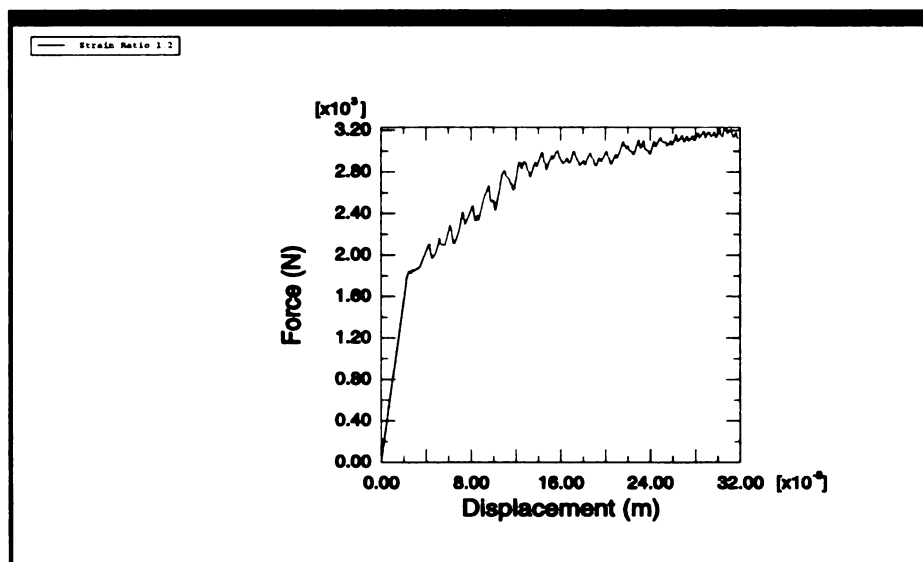Figure 5.9: Deformed shape, Strain Ratio = 4.8
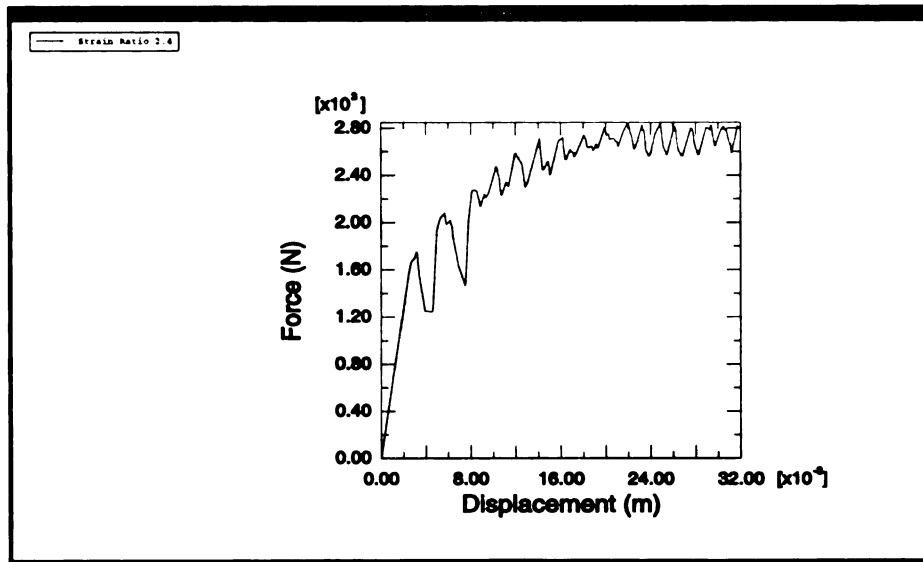

Figure 5.10: Force vs Displacement, Strain Ratio = 1.2

80

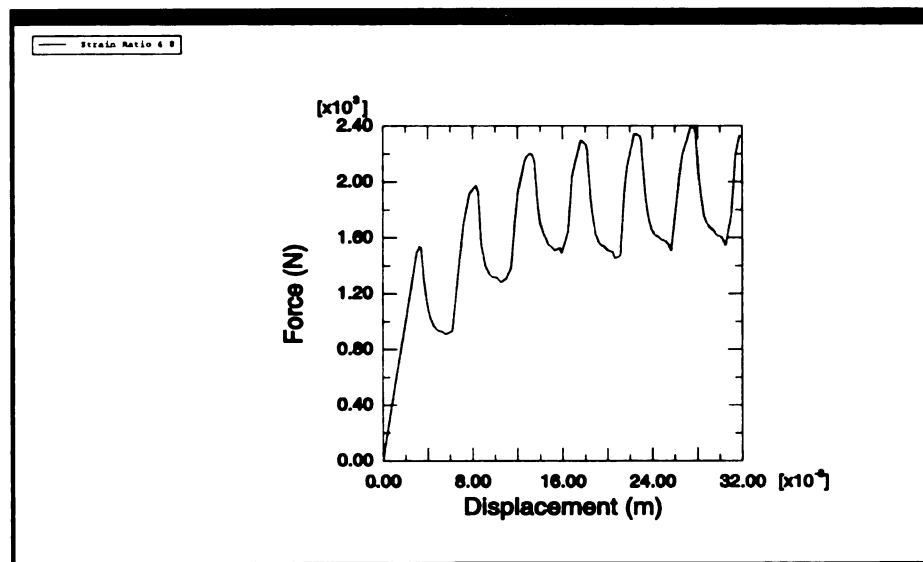Figure 5.11: Force vs Displacement, Strain Ratio = 2.4

Figure 5.12: Force vs Displacement, Strain Ratio = 4.8

81

In Table 5.5, error in the Energy absorbed (compared to Energy Absorbed for a Strain Ratio of 1.2), and the improvement in number of increments required to complete the analysis is tabulated for several values of Strain Ratio. Figure 5.13 is a graphical representation of the same data. For a Strain Ratio 1.3, the error in the Energy absorbed is 8.43% while there is a 35% reduction in the number of increments required to complete the analysis and a 22% reduction in time required to complete the analysis.

SR	Response, (J)	No. of Increments	Hrs. to complete	Strength, MPa	Error in Response, %	% Improvement in No. of Inc.	% Improvement in time
1.2	84	5833	7.7	155	0	0	0
1.3	76.92	3846	6.00	148.919	8.43	34.06	22.08
1.4	75.19	3318	5.5	143.502	10.49	43.12	28.57
1.5	76.31	3189	4.25	138.6362	9.16	45.33	44.81
1.6	74.22	2793	3.17	134.233	11.64	52.12	58.87
2.0	76.86	3012	4.5	120.062	8.5	48.36	41.56
2.4	73	2837	2.5	109.655	13.10	51.36	67.53
2.8	70	2521	3.42	101.47	16.67	56.78	55.63
3.2	68.33	2567	3.42	94.9177	18.65	55.99	55.63
3.6	62.48	2130	3.25	89.489	25.62	63.48	57.79
4.0	62.16	2128	3.00	84.896	26.0	63.52	61.04
4.4	63.94	1376	2.0	80.946	23.88	76.41	74.03
4.8	51	1998	1.66	77.5	39.29	65.75	78.44

Table 5.5: Effect of Strain Ratio, (Detail)

It is true that number of increments is not the best representation for the convergence rate nor is it directly proportional to the time required to complete the analysis. This is because each increment may have different number of iterations depending on whether the guessed solution is within the convergence radius. The trend that has been established in
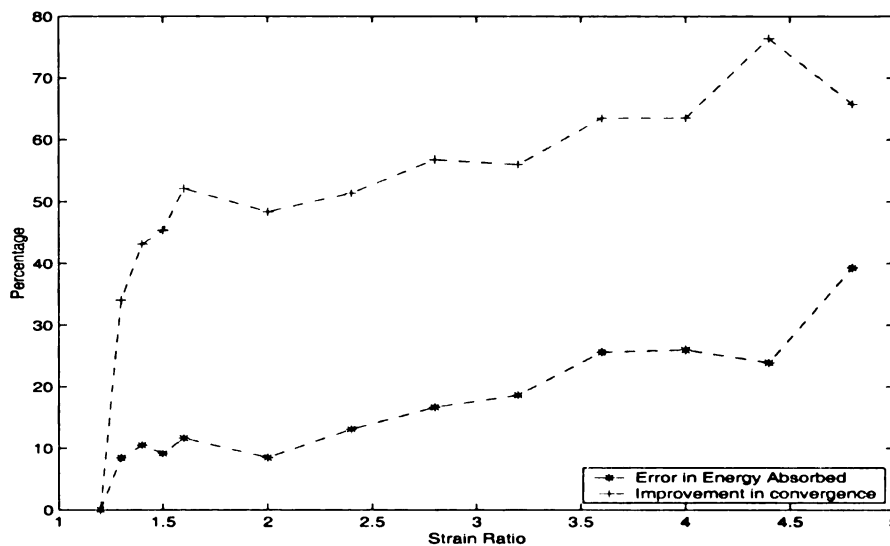
Figure 5.13: Improvement in convergence through high Strain Ratio

this study only indicates that it is possible to obtain quicker converged solution with a lower sacrifice in the accuracy of the response (Energy Absorbed), with a careful choice of the Strain Ratio.

5.3 Conclusion

As a result of the work done, it is evident that obtaining responses for quasi-static crush problems is very challenging due to high degree of non-linearity. However , "localization limiters" like visco plastic algorithm come to our rescue and help to obtain meaningful solutions with some effort. Convergence due to contact may be overcome by having a finer mesh for the slave surface than the master surface (please see Figure 3.3.1 .

ANOVA results enable us to conclude that delamination is a significant factor affecting the response. It decreases the overall stiffness of the tube and decreases the energy that can be absorbed by the tube. Numerical modeling of delamination is crucial to accurately represent failure of composite tubes during crushing. Factors like friction contribute to nearly 50% of the total energy absorbed and this is consistent with the literature [2] and [3]. Other factors like friction between plies and the RDR factor do not affect the response in this case. Use of several plies may lead to a different conclusions for these factors.

5.4 Scope for future Research

As described, ANOVA was done using *Ms Excel* and all the analysis needed to be carried out separately from the command prompt. It is also possible to automate the process using softwares. This was attempted in this work using a software called HEEDS (Heirarchial Evolutionary Engineering Design System) developed at Red Cedar Technology, East Lansing, Michigan, for advanced optimization problems. HEEDS is also capable of performing ANOVA once the variables (*Factors*) and their *levels* are specified. HEEDS allows the user to *tag* the design variables and the *response*. The user can also specify a tool or many tools that will be used to evaluate the design and output the response. Once all such evaluations are carried out HEEDS writes out in an output file the contribution of each effect. All factors except delamination (*presence and absence*) are quantitative and can be directly *tagged*, to set up the problem in HEEDS. The delamination factor can be implemented using the methods described in sections 4.4.2 and 4.5.3, by varying the strength of the interface strength to effect delamination. This work may be extended to perform advanced ANOVA studies using HEEDS.

Though convergence and mesh sensitivity are crucial problems in softening material models in numerical analysis , methods to overcome these can be implemented in material models used to simulate failure in composite structures. Some methods available for this purpose are suggested and explained in [18, 21–23]. As a motivation for furthering improvement in building material models involving softening it should be interesting and useful to incorporate concepts of "localization limiters" and objective methods of specifying the softening behavior.

BIBLIOGRAPHY

[1] A penalty based interface technology for connecting independently modeled substructures for simulation growth of delamination in composite structures, by Dr. Antonio Pantano and Dr. Ronald C. Averill.

[2] Mamalis, A. G., Manolakos, D. E., Demosthenous, G. A., Ioannidis, M. B., Crashworthiness of composite Thin-Walled structural Components. *Technomic Publishing Co., INC.* Lancaster Basel.

[3] Mamalis, A. G., Manolakos, D. E., Demosthenous, G. A., Ioannidis, M. B., The Static and Dynamic Axial Crumbling of thin walled fiberglass composite square tubes. *Composites Part B*, **28B**(1997), 439-451.

[4] Abdel-Haq, M and Newaz, G. M., Role of Failure Modes on Energy absorption in Unidirectional PMC Tubes. *Journal of Composite Materials*, **Vol. 35**, No.11/2001.

[5] Yuan, Y. B., Vlegelahn, G. L., Modeling of Crushing Behavior of Fiberglass/Vinylester Tubes. *Advanced Composite Materials: New Developments and Applications Conference Proceedings, Detroit, Michigan USA Sept. 30 - Oct. 3, 1991.*

[6] Gary L.Farley and Robert M. Jones, Analogy for the effect of Material and Geometrical Variables on Energy-Absorption Capability of Composite tubes. *Journal of Composite Materials*, **Vol. 26**, No. 1/1992.

[7] Scott Burr, Daryl Hertema, Jeff Sweeney, Taking a hit:- Modeling the parameters of thermoplastics in car crashes. *Plastics Engineering*, **September '97**.

[8] Mamalis, A. G., Monolakos, D. E., Demosthenous, G. A., Ioannidis, M. B., Axial Collapse of thin-walled fiberglass tubular composite components at elevated strain rates. *Composites Engineering*, **3**, 1994.

[9] Mamalis, A. G., Yuan, Y. B., Viegelahn, G. I., Collapse of thin walled composite sections subjected to high speed axial loading. *International Journal of Vehicle Design*, 1992, **13**, 564.

[10] Hannapel, F. W., Yuan, Y. B., Vlegelahn, G. L., Martin. C. D., Crashworthy characteristics of fiberglass/polyester frusta under quasi-static axial loading. *Advanced Composite Materials: New Developments and Applications Conference Proceedings, Detroit, Michigan USA*, **Sept. 30-Oct. 3, 1991.**

[11] Shu Ching Quek, Anthony M.Waas, Jennifer Hoffman, Venkatesh Agaram, The Crushing Response of braided and CSM glass reinforced composite tubes. *Composite Structures*, **Vol. 52**, 2001, 103-112.

[12] David C. Flemming, Modeling delamination growth in composites using MSC Dytran.

[13] Shawn J. Beard, Energy absorption of braided composite tubes, *A Dissertation submitted to the department of aeronautics and astronautics and the committee on graduate studies of Stanford University*, April 2001.

[14] Ronald Krueger , Pierre J. Minuguet and T. Kevin O'Brien, A method for calculating Strain Energy Release Rates in preliminary design of composite skin/stringer debonding under multi-axial loading. *Composite Structures: Theory and Practice, ASTM STP 1383, 2000, pp. 105-128.*

[15] Gary L.Farley and Robert M. Jones, Prediction of energy absorption capability of composite tubes. *Journal of Composite Materials*, **Vol, 26**, No. 3/1992.

[16] E.Haug & A. De Rouvray, Crash Response of Composite Structures. *Engineering Systems International SA, 94578 Rungis-Cedex, France*

[17] Don Simons, Constitutive Model V & V for softening Materials.

[18] Zdenek P. Basant and Jaime Planas, Fracture and Size effect in concrete and other Quasi-brittle Materials. *CRC Press*

[19] *State of the Art Report on Finite element Analysis of Reinforced Concrete.* Published by American Society of Civil engineers.

[20] Hibbit, Karlsson, & Sorenson, ABAQUS *V 6.3* Manuals.

[21] Etse, G, William, K., Failure Analysis of Elasto–Viscoplastic Material Models. ASCE *Journal of Engineering Mechanics*, **Vol 125**, 1999, 60–69.

[22] Milan Jirásek, Zdenek P. Bazant., Inelastic Analysis of Structures. *John Wiley & Sons*; (November 12, 2001) .

[23] Needleman, A., Material rate dependence and mesh sensitivity in localization problems. *Comp. Meth. Appl. Mech. and Engineering*, Vol 63, 1988, 69–85.

[24] Hillerborg. A., Modeer. M., Peterson, P. E., Analysis of crack formation and crack growth in concrete by means of fracture mechanics and Finite Elements. *Cement and Concrete Research*, Vol. 6, 1976, pp. 773-782.

[25] J. N. Reddy, An introduction to the Finite Element Method-2nd ed. *McGraw-Hill series in Mechanical Engineering*.

[26] Douglas C. Montgomery, Design and Analysis of experiments. *John Wiley & Sons, INC*.

[27] T. Kevin O' Brein. Characterization, Analysis and Prediction of Delamination in Composites using fracture Mechanics.*Oral Reference number : ICF100942OR*

[28] J. N. Reddy, Energy and Variational methods in Applied Mechanics. *A Wiley-Interscience Publication*, John Wiley & Sons.

[29] Dr. Robert M. Jones, Mechanics of Composite Materials. *Taylor & Francis*

[30] Alastair F. Jhonson and Anthony K. Pickett, Impact and Crash modeling of Composite Structures: A challenge for Damage Mechanics.

[31] P. Ladeveze and E Le Dantec, Damage Modeling of the Elementary ply for laminated composites. *Composites Science and Technology*, Vol. 43, No. 3/1992, pp 257-267.

[32] Kupfer, H., Hilsdorf, H.K., Rusch, K., Behavior of concrete under biaxial stresses. *Journal of the American Concrete Institute*, Vol. 66, No.8, August 1969, pp. 656-666

[33] Chen, W. F., Plasticity in Reinforced Concrete. *McGraw Hill*, (January 1982).

[34] Sultan T. Mesmar, Roger S. Crouch, Fracture Regularization by extension of the explicit microplane model for concrete to include Duvaut-Lions visco-plasticity by, *European Congress on Computational Methods in Applied Seiences and Engineering*,

ECOMAS 2000.

[35] Computational Inelasticity by Simo and Hughes. *Springer Verlag*, (August 1998).

[36] Anderson, T. L., Fracture Mechanics, Fundamentals and Applications, *CRC Press*.

[37] Leslie M. Moore and Bonnie K. Ray, Statistical methods for sensitivity and perfor-mance analysis in computer experiments. *Proceedings of the 1999 Winter Simulation Conference.*

[38] Jerome Sacks ,Susannah B. Schiller and William J. Welch, Design of Computer Ex-periments. *Technometrics, Feb. 1989*, **Vol. 31**, No. 1.

[39] William J. Welch, Robert J. Buck, Jerome Sacks, Henry P. Wynn, Toby J. Mitchell and Max D. Morris, Screening, predicting and Computer Experiments. *Technometrics, February 1992*, **Vol. 34**, No. 1.

[40] Lubliner, J., J. Oliver, S. Oller and Oñate, A Plastic- Damage model for concrete. *International Journal of Solids and Structures* ,**Vol. 25**, No. 3, pp 229-326, 1989.

[41] Lee, J., and G. L. Fenves, Plastic Damage Model for Cyclic loading of Concrete Structures. *Journal Of Engineering Mechanics*, **Vol. 124**, No. 8, pp, 892-900, 1998

[42] Tim Rzenitzek, Dr. Heiner Müllerschön, Dr. Frank C. Günther and Michal Wozniak, Two-stage Stochastic and Deterministic Optimization.

[43] MI. Y, Crisfield, M. A., Davies, G. A. O., and Hellweg, H. B., Progressive Delamina-tion Using Interface Elements. *Journal of Composite Materials*, **Vol. 32**, No. 14/1998.

[44] Xianqiang Lu and Dahsin Liu, Finite Element Analysis of Strain Energy Release Rate at Delamination Front. *Journal of Reinforced Plastics and Composites*, **Vol. 10**, May 1991.

[45] Bruno. D, Greco. F, Lonetti. P, Modeling of delamination and contact in composite laminates.

[46] Reedy. Jr, E. D., Mello F. J., Guess. T. R., Modeling the initiation and growth of delaminations in composite structures. *Journal of composite materials*, **Vol 31**, No. 8, 1997, pp. 812 - 831.

[47] Hull, D, A unified approach to progressive crushing of fiber-reinforced composite tubes. *Composite Science and technology*, **Vol. 40**, (1991), 377-421.

[48] Vreede, P. T., Van Veldhuizen, Kragtwijk, S. P., Carleer, B. B, Finite Element analysis of tubular energy absorber in automobiles. *University of Twente, Enschede*, The Netherlands.

[49] Ribeaux, M, Warrior, N. A., Effect of Impact Damage on the Specific Energy Absorption of Glass/Polyster Composites. *University of Nottingham, NG7 2RD UK*.